SURFACE REFLECTANCE

VISIBLE/INFRARED IMAGER/RADIOMETER SUITE
ALGORITHM THEORETICAL BASIS DOCUMENT
Version 4: May 2001

Shawn W. Miller

Eric Vermote (University of Maryland), Science Team Member

RAYTHEON ITSS
4400 Forbes Boulevard
Lanham, MD 20706

SBRS Document #: Y2411

Product: SURFACE REFLECTANCE IP

Doc No: Y2411

Version: 4

Revision: 0

	Function	Name	Signature	Date
Prepared by	IP Developer	S. MILLER		
Approved by	Relevant IPT Lead	S. MILLER		
Reviewed by	Reviewer	K. JENSEN		
Approved by	Chief Scientist	S. MILLER		
Released by	Algorithm Lead	P. KEALY		

Raytheon

TABLE OF CONTENTS

Raytheon

LIST OF FIGURES

Raytheon

LIST OF TABLES

Raytheon

GLOSSARY OF ACRONYMS

3D	Three Dimensional
6S	Second Simulation of the Satellite Signal in the Solar Spectrum
AERONET	Aerosol Robotic Network
AOT	Aerosol Optical Thickness
ASAS	Advanced Solid-state Array Spectroradiometer
ASTER	Advanced Spaceborne Thermal Emission and Reflection Radiometer
ATBD	Algorithm Theoretical Basis Document
AVHRR	Advanced Very High Resolution Radiometer
BBR	Band to Band Registration
BRDF	Bidirectional Reflectance Distribution Function
BOREAS	Boreal Ecosystem/Atmosphere Study
CMIS	Conical-scanning Microwave Imager/Sounder
CrIS	Cross-track Infrared Sounder
DEM	Digital Elevation Model
DISORT	Discrete Ordinates Radiative Transfer Model
DoD	Department of Defense
EDR	Environmental Data Record
EOS	Earth Observing System
ETM+	Enhanced Thematic Mapper +
EVI	Enhanced Vegetation Index
FWHM	Full Width Half Maximum
GIFOV	Ground Instantaneous Field of View
GSD	Ground Sample Distance
GTOS	Global Terrestrial Observing System
HSI	Horizontal Sample Interval
HSR	Horizontal Spatial Resolution
IFOV	Instantaneous Field of View
ICD	Interface Control Document
I/O	Input/Output
IP	Intermediate Product
IPO	Integrated Program Office

LLLS	Low-level Light Sensor
LOWTRAN	Low Resolution Atmospheric Radiance and Transmittance Model
LQF	Land Quality Flag(s)
LTER	Long Term Ecological Research
LUT	Lookup Table
MMNSR	Monthly Mean Non-Snow Reflectance
MODIS	Moderate Resolution Imaging Spectroradiometer
MODTRAN	Moderate Resolution Atmospheric Radiance and Transmittance Model
MSR	Monthly Surface Reflectance
MTF	Modulation Transfer Function
NASA	National Aeronautics and Space Administration
NCEP	National Centers for Environmental Prediction
NDVI	Normalized Difference Vegetation Index
NOAA	National Oceanic and Atmospheric Administration
NOGAPS	Navy Operational Global Atmospheric Prediction System
NPOESS	National Polar-orbiting Operational Environmental Satellite System
NPP	NPOESS Preparatory Project
OLS	Optical Line Scanner
OMPS	Ozone Mapping Profiling Suite
PARABOLA	Portable Apparatus for Rapid Acquisition of Bidirectional Observations of Land and Atmosphere
POLDER	Polarization and Directionality of the Earth's Reflectances
QC	Quality Control
RDR	Raw Data Record
RMS	Root Mean Square
RSR	Relative Spectral Response
RT	Radiative Transfer
SBRS	Santa Barbara Remote Sensing
SDP	Science Data Processing
SDR	Sensor Data Record
SDSM	Solar Diffuser Stability Monitor
SeaWiFS	Sea-viewing Wide Field-of-view Sensor
SNR	Signal to Noise Ratio

Raytheon

SOS	Successive Order of Scattering
SRD	Sensor Requirements Document
SWIR	Short Wave Infrared
SZA	Solar Zenith Angle
TBD	To Be Determined
TERCAT	Terrain Categorization
THEMIS	Thermal Emission Imaging System
TIROS	Television/Infrared Observation Satellite
TM	Thematic Mapper
TOA	Top of Atmosphere
TOC	Top of Canopy
VCM	VIIRS Cloud Mask
VIIRS	Visible/Infrared Imager Radiometer Suite
VNIR	Visible/Near Infrared
VOAT	VIIRS Operational Algorithm Team
VZA	View Zenith Angle
WSR	Weekly Surface Reflectance

ABSTRACT

The algorithm described in this document produces the Surface Reflectance Intermediate Product (IP), one of over thirty products to be generated from the National Polar-orbiting Operational Environmental Satellite System (NPOESS) Visible/Infrared Imager/Radiometer Suite (VIIRS), scheduled for launch late in the first decade of the 21st century. The VIIRS prototype will be carried onboard the NPOESS Preparatory Project (NPP) spacecraft to be launched by the National Aeronautics and Space Administration (NASA) in 2005.

The Surface Reflectance IP consists of directional surface reflectances in bands centered at 0.412 μm, 0.445 μm, 0.488 μm, 0.555 μm, 0.645 μm, 0.672 μm, 0.865 μm (two different spatial resolutions), 1.24 μm, 1.61 μm (two different spatial resolutions), and 2.25 μm. The algorithm corrects for the effects of gaseous absorption, molecular and aerosol scattering, thin cirrus contamination, and the coupling of the atmosphere and the surface bidirectional reflectance, using a lookup table (LUT) based upon a radiative transfer model (e.g., MODTRAN, 6S, etc.). The correction uses aerosol information from VIIRS aerosol Environmental Data Records (EDRs), complemented by: water vapor from VIIRS, National Center for Environmental Prediction (NCEP) feeds, or the Conical-scanning Microwave Imager/Sounder (CMIS); cirrus cloud optical properties from VIIRS; surface pressure for Rayleigh scattering correction from NCEP; and column ozone from the Ozone Mapping Profiling Suite (OMPS). The correction also uses a surface Bidirectional Reflectance Distribution Function (BRDF)/albedo model for correcting the coupled atmospheric and surface anisotropic effects. Once handling of adjacency effects have reached a sufficient level of maturity, these will also be explicitly accounted for by the VIIRS algorithm.

This document presents the theoretical basis of the Surface Reflectance algorithm, adapted from the analogous Moderate Resolution Imaging Spectroradiometer (MODIS) algorithm theoretical basis (Vermote and Vermeulen, 1999). It also discusses uncertainties due to errors in the algorithm and its multiple input parameters. Sensitivity studies conducted thus far indicate that the major error source in the surface reflectance retrieval is that associated with the retrieval of tropospheric aerosol properties. Further sensitivity studies will lead to a refinement of the LUT, and a separation of as many of its dimensions as possible into separate empirical formulae or correction factors, leading to a streamlined operational algorithm.

Raytheon

1.0 INTRODUCTION

1.1 PURPOSE

This Algorithm Theoretical Basis Document (ATBD) describes the algorithms used to retrieve the Surface Reflectance Intermediate Product (IP) from Visible/Infrared Imager/Radiometer Suite (VIIRS) measurements. It identifies the sources of input data, both VIIRS and non-VIIRS, that are required for Surface Reflectance retrievals. It provides the physical theory and mathematical background underlying the approach, and it includes top-level implementation details. The VIIRS Science Data System Team is using information continued in this document to establish the requirements and functionality of the data processing software.

1.2 SCOPE

This document covers the algorithm theoretical basis for the Surface Reflectance IP. Other post-launch products are not discussed in any detail. For a detailed discussion of software implementation, the reader is directed to *[Y2469], [Y2474], [Y2483], and [Y2498]*. The algorithms for producing gridded derived products directly from the Surface Reflectance IP are described in *[Y7051]*.

Section 1 of this ATBD describes the purpose and scope of the document. Section 2 provides an overview of the experiment. The processing concept and algorithm description are presented in Section 3. Section 4 summarizes assumptions and limitations, and references for publications cited in the text are provided in Section 5.

1.3 VIIRS DOCUMENTS

References to VIIRS documents will be indicated by Raytheon Santa Barbara Remote Sensing (SBRS) official Y-numbers in italicized brackets, e.g., *[Y2388]*.

Y2387 VIIRS Soil Moisture ATBD

Y2388 VIIRS Aerosol Optical Thickness and Particle Size ATBD

Y2390 VIIRS Suspended Matter ATBD

Y2393 VIIRS Cloud Effective Particle Size and Cloud Optical Thickness ATBD

Y2398 VIIRS Surface Albedo ATBD

Y2400 VIIRS Vegetation Index ATBD

Y2401 VIIRS Snow Cover/Depth ATBD

Y2402 VIIRS Surface Type ATBD

Y2404 VIIRS Fresh Water Ice ATBD (product is pending cancellation)

Y2409 VIIRS Sea Ice Age/Edge Motion ATBD

Y2412 VIIRS Cloud Mask ATBD

Y2466 VIIRS Imagery ATBD

Y2468 VIIRS Operations Concept Document

Y2469 VIIRS Context Level Software Architecture

Y2470 VIIRS Interface Control Document

Y2474 VIIRS Land Module Level Software Architecture

Y2483 VIIRS Land Module Level Detailed Design Document

Y2498 VIIRS Surface Reflectance IP Unit Level Detailed Design Document

Y3236 VIIRS Software Integration and Test Plan

Y3237 VIIRS Algorithm Verification and Validation Plan

Y3251 VIIRS Precipitable Water ATBD

Y3252 VIIRS Active Fires ATBD

Y3257 VIIRS Computer Resources Requirements Document

Y3261 VIIRS Radiometric Calibration ATBD

Y3270 VIIRS System Verification and Validation Plan

Y3279 VIIRS Land Module Level Interface Control Document

Y6635 VIIRS Algorithm Software Development Plan

Y6661 VIIRS Algorithm Software Maturity Assessment

Y7040 VIIRS Algorithm/Data Processing Technical Report

Y7051 VIIRS Earth Gridding ATBD

SS154650 VIIRS System Specification

PS154650 VIIRS Sensor Specification

PS154640 VIIRS Algorithm Specification

1.4 REVISION HISTORY

This is the fourth version of this document, dated May 2001. The third version was dated May 2000. The second version was dated June 1999. The first version was dated October 1998. The author would like to thank Wenge Ni for extensive contributions to earlier versions of this document, and also Alexei Lyapustin and Eric Vermote for numerous insightful discussions of the theoretical basis presented here. This document has received extensive revisions since Version 3. It has been modified in the following general areas:

1) Movement to a more generic treatment of RT modeling

2) Generalization of all the important inputs into lookup table (LUT) dimensions (this is a step back to allow an abbreviated reassessment of the structure of the LUT and the relative importance of each of the Surface Reflectance IP inputs

3) Addition of new sensitivity analyses to start the process of refining the lookup table (LUT) and convert as many dimensions as possible into correction factors or empirical formulae

4) Refinement of quality flag strategy, which will be detailed even further in Version 5 of this ATBD

5) Updated VIIRS band names

6) Further refinement of gridded products derived from the Surface Reflectance IP (more detail can be found in *[Y7051]*

7) Addition of a thin cirrus correction methodology, which will be significantly refined in Version 5 of this ATBD.

2.0   EXPERIMENT OVERVIEW

2.1   OBJECTIVES OF SURFACE REFLECTANCE RETRIEVALS

A number of VIIRS products require surface reflectances as input. These include: Surface Albedo *[Y2398]*; Soil Moisture *[Y2387]*; top-of-canopy (TOC) Enhanced Vegetation Index (EVI) and Normalized Difference Vegetation Index (NDVI), both described in *[Y2400]*; Surface Type *[Y2402]*; Snow Cover/Depth *[Y2401]*; Imagery for sea ice applications *[Y2466]*; and Sea Ice Age/Edge Motion *[Y2409]*. The signal at the top of the atmosphere in a given VIIRS spectral band will contain information about both the surface and the atmosphere; the latter information must be removed to facilitate successful retrievals of the products listed above. Further, the products listed above feed into one another and into other VIIRS products, such as Leaf Area Index (LAI, *[Y2400]*) and Active Fires *[Y3252]*. It is therefore vital to derive an intermediate product (IP) for VIIRS that contains directional surface reflectances in all the relevant bands. In recognition of this, Raytheon adopted the MODIS surface reflectance algorithm, described in Vermote and Vermeulen (1999), as the baseline VIIRS approach during Phase I algorithm development, which concluded in the spring of 2000. Phase II algorithm development, which commenced in the winter of 2000, has led to further refinements in the algorithm theoretical basis. The latest version of the VIIRS Sensor Requirements Document (SRD, IPO [2000]) explicitly requires directional surface reflectances as part of the derivation of the Surface Albedo Environmental Data Record (EDR), however the Surface Reflectance IP will remain a distinct product within the VIIRS processing architecture, and the ATBD will be kept separate as well. The V4 algorithms for Surface Albedo and Vegetation Index use top-of-atmosphere (TOA) reflectances instead of surface reflectances under some circumstances. Retrieval of TOA reflectance is described in *[Y3261]*.

Operational implementation of this algorithm requires the use of a look-up table (LUT) based on radiative transfer (RT) modeling. Candidate models for providing the RT basis to the LUT include but are not limited to MODTRAN 4.0 (Berk *et al.*, 1999) and the Second Simulation of the Satellite Signal in the Solar Spectrum (6S) developed at the Laboratoire d'Optique Atmospherique of Lille, France (Vermote *et al.,* 1995, 1997). A generic LUT generation tool is being developed by Raytheon to maximize the flexibility of this and other LUTs in the VIIRS algorithm subsystem.

2.2   INSTRUMENT CHARACTERISTICS

The VIIRS instrument is now briefly described to clarify the context of the descriptions of the Surface Reflectance IP presented in this document. VIIRS can be pictured as a convergence of three existing sensors, two of which have seen extensive operational use at this writing.

The Operational Linescan System (OLS) is the operational visible/infrared scanner for the Department of Defense (DoD). Its unique strengths are controlled growth in spatial resolution through rotation of the ground instantaneous field of view (GIFOV) and the existence of a low-level light sensor capable of detecting visible radiation at night. OLS has primarily served as a data source for manual analysis of imagery. The Advanced Very High Resolution Radiometer (AVHRR) is the operational visible/infrared sensor flown on the National Oceanic and Atmospheric Administration (NOAA) Television InfraRed Observation Satellite (TIROS-N)

series of platforms (Planet, 1988). Its unique strengths are low operational and production cost and the presence of five spectral channels that can be used in a wide number of combinations to produce operational and research products. In December 1999, the National Aeronautics and Space Administration (NASA) launched the Earth Observing System (EOS) morning satellite, *Terra*, which includes the Moderate Resolution Imaging Spectroradiometer (MODIS). This sensor possesses an unprecedented array of thirty-two spectral bands at resolutions ranging from 250 m to 1 km at nadir, allowing for currently unparalleled accuracy in a wide range of satellite-based environmental measurements.

VIIRS will reside on a platform of the National Polar-orbiting Operational Environmental Satellite System (NPOESS) series of satellites. It is intended to be the product of a convergence between DoD, NOAA and NASA in the form of a single visible/infrared sensor capable of satisfying the needs of all three communities, as well as the research community beyond. As such, VIIRS will require three key attributes: high spatial resolution with controlled growth off nadir; minimal production and operational cost; and a sufficient number of spectral bands to satisfy the requirements for generating accurate operational and scientific products.

Figure 1 illustrates the design concept for VIIRS, designed and built by Raytheon Santa Barbara Remote Sensing (SBRS). At its heart is a rotating telescope scanning mechanism that minimizes the effects of solar impingement and scattered light. VIIRS is essentially a combination of SeaWiFS foreoptics and an all-reflective modification of MODIS/THEMIS aft-optics. Calibration is performed onboard using a solar diffuser for short wavelengths and a blackbody source and deep space view for thermal wavelengths. A solar diffuser stability monitor (SDSM) is also included to track the performance of the solar diffuser. The nominal altitude for NPOESS will be 833 km. The VIIRS scan will therefore extend to 56 degrees on either side of nadir.

The VIIRS Sensor Requirements Document (SRD, IPO [2000]) places explicit requirements on spatial resolution for the Imagery Environmental Data Record (EDR). Specifically, the horizontal spatial resolution (HSR) of bands used to meet threshold Imagery EDR requirements must be no greater than 400 m at nadir and 800 m at the edge of the scan. This led to the development of a unique scanning approach which optimizes both spatial resolution and signal to noise ratio (SNR) across the scan. The concept is summarized in Figure 2 for the imagery bands; the nested lower resolution radiometric bands follow the same paradigm at approximately twice the size. The VIIRS detectors are rectangular, with the smaller dimension along the scan. At nadir, three detector footprints are aggregated to form a single VIIRS "pixel." Moving along the scan away from nadir, the detector footprints become larger both along track and along scan, due to geometric effects and the curvature of the Earth. The effects are much larger along scan. At around 32 degrees in scan angle, the aggregation scheme is changed from 3x1 to 2x1. A similar switch from 2x1 to 1x1 aggregation occurs at 48 degrees. The VIIRS scan consequently exhibits a pixel growth factor of only 2 both along track and along scan, compared with a growth factor of 6 along scan which would be realized without the use of the aggregation scheme. Figure 3 illustrates the benefits of the aggregation scheme for spatial resolution. HSI stands for horizontal sampling interval, the distance between centers of aggregated pixels along-scan. GSD is the ground sample distance between individual detector footprints.

Raytheon
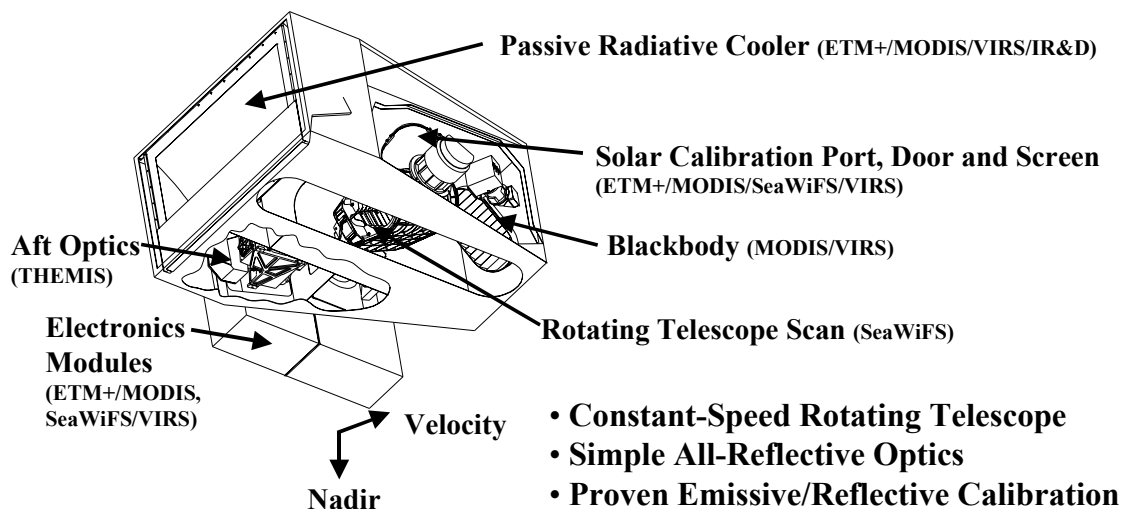
Figure 1. Summary of VIIRS design concepts and heritage.

Fine-Resolution Bands
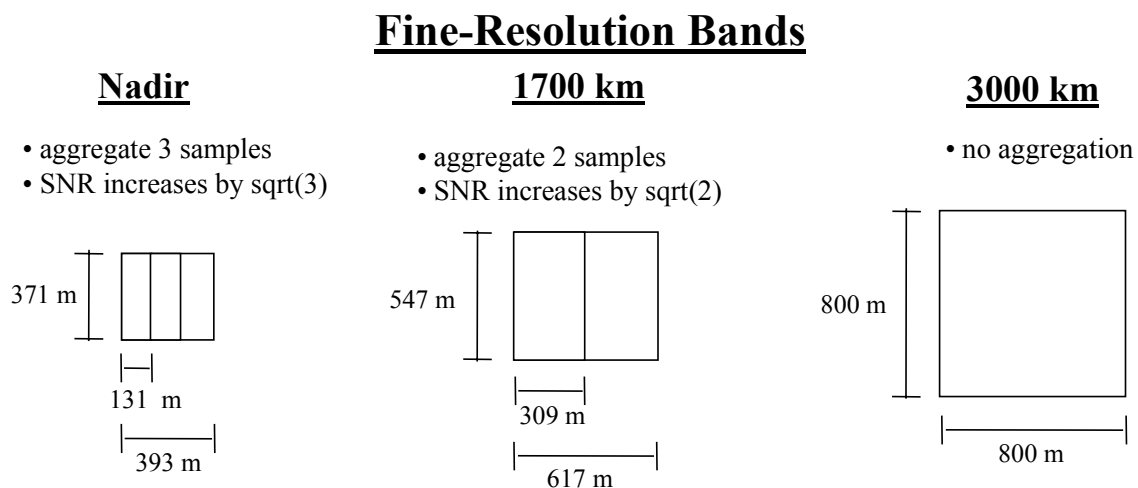
Figure 2. VIIRS detector footprint aggregation scheme for building "pixels."

Scan HSI as a Function of Scan Angle
for Unit Raw GSD at Nadir
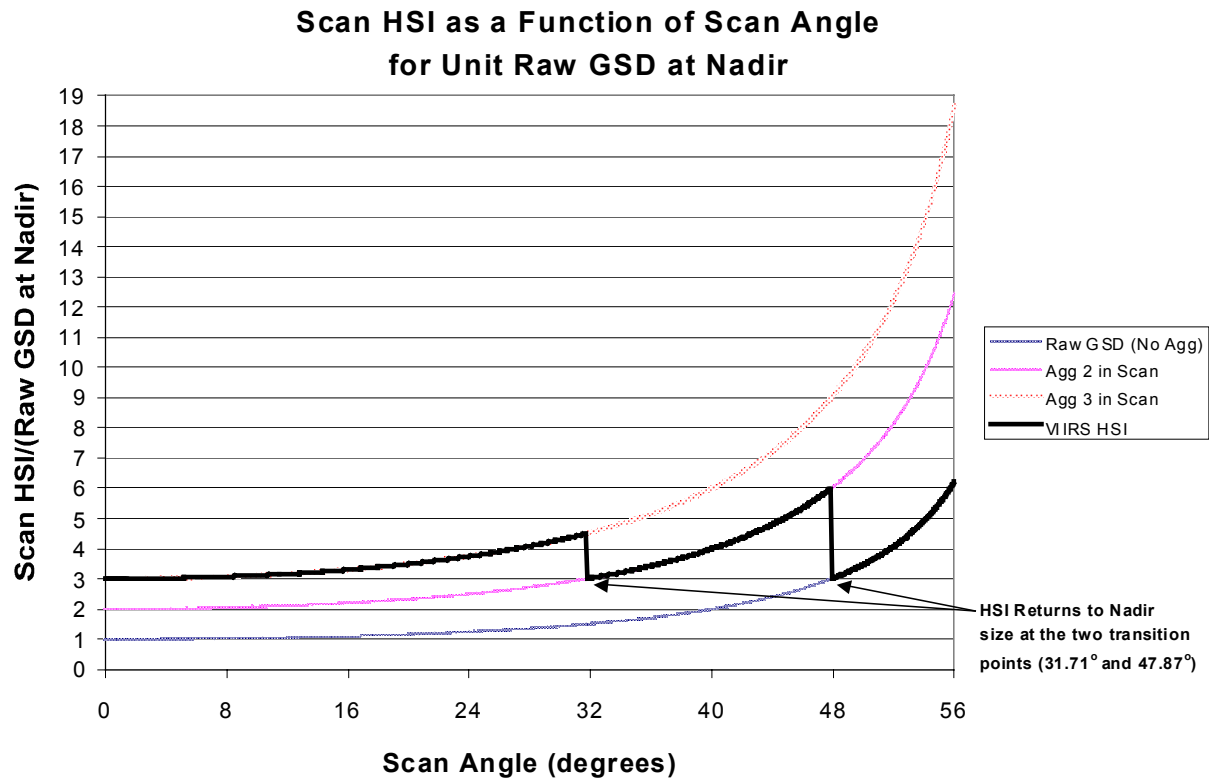
Figure 3. Benefits of VIIRS aggregation scheme in reducing pixel growth at edge of scan.

This scanning approach is extremely beneficial for the retrieval of land products such as the NDVI. The increasing importance of land cover change detection makes high spatial resolution in the NDVI and its input reflectances much more important; by comparison, signal to noise ratio (SNR) is a secondary issue (this latter point will be verified later in this document).

The positioning of the VIIRS Visible/Near Infrared (VNIR) and Short Wave Infrared (SWIR) spectral bands is summarized in Figure 4 and Figure 5. The radiometric, spatial, and spectral performances of these bands are summarized in the VIIRS Sensor Specification *[PS154650]*.
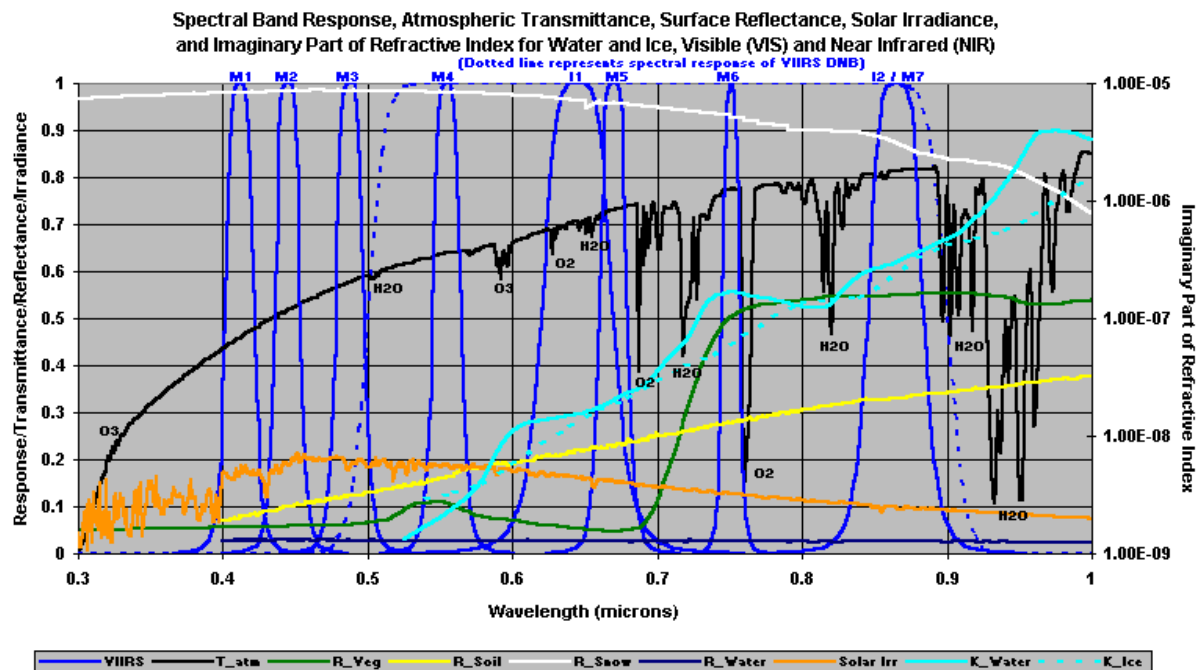
Figure 4. VIIRS spectral bands, visible and near infrared.
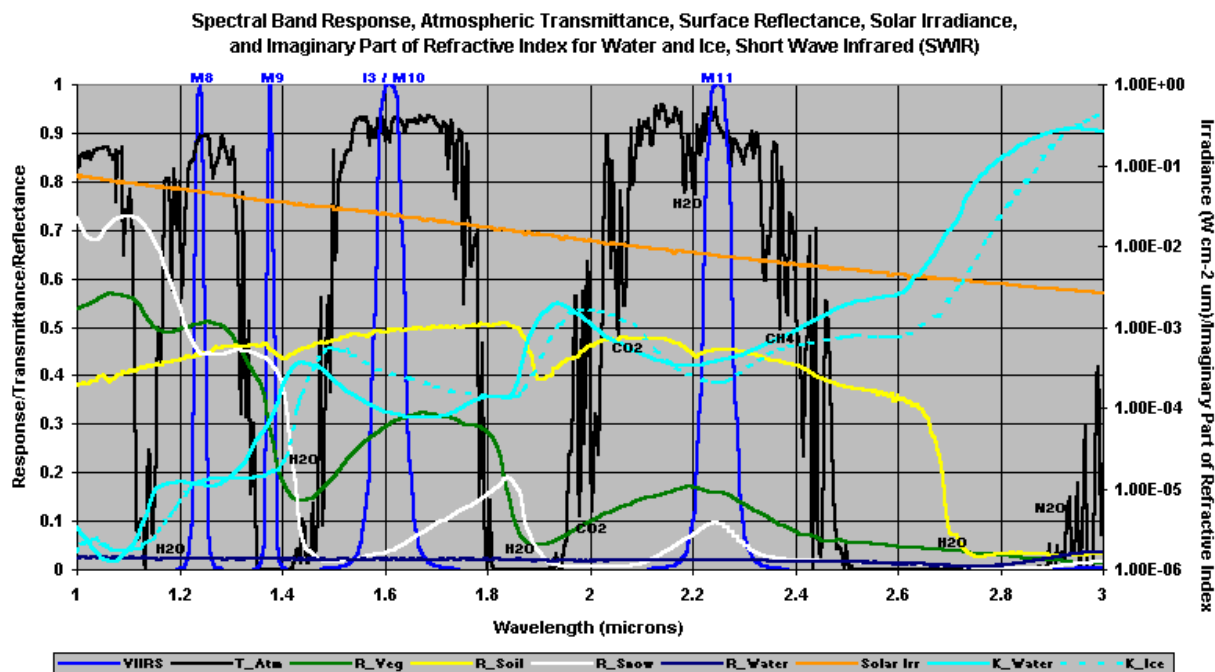
Figure 5. VIIRS spectral bands, short wave infrared.

2.3 RETRIEVAL STRATEGY

Retrievals of the Surface Reflectance IP will be conducted for all clear daytime pixels within the array of NPOESS/VIIRS swaths. A product will also be generated for pixels contaminated by correctable thin cirrus, defined by a threshold optical depth to be determined (TBD). Retrievals will be conducted over both land and ocean, as the Surface Albedo EDR for dark surfaces requires Surface Reflectance as input, and this product must be retrieved globally. "Daytime" here is defined by a local solar zenith angle of 85 degrees or less. The performance specification for Surface Reflectance is not presently guaranteed all the way out to this limit. "Clear" is defined by a specification of "probably cloudy", "probably clear," or "confident clear" for the relevant Cloud Mask tests, which will be identified and discussed in Version 5 of this document.

Once a pixel has been qualified for retrieval, the Surface Reflectance LUT is implemented using: the VIIRS Calibrated Radiances SDR *[Y3261]*; the VIIRS Aerosol Optical Thickness EDR *[Y2388]*; the VIIRS Suspended Matter EDR *[Y2390]*; the VIIRS Cloud Effective Particle Size and Cloud Optical Thickness EDRs *[Y2393]*; the VIIRS Precipitable Water EDR *[Y3251]*; the VIIRS Surface Types—Biomes IP *[Y2402]*; column ozone from the NPOESS Ozone Mapping Profiling Suite (OMPS); and surface pressure from NCEP analyses. Aerosol optical thickness and type, cirrus cloud optical thickness and particle size, column water vapor, column ozone, TOA radiances, and solar/viewing geometry are baseline inputs to the LUT. Surface pressure and elevation are required for a Rayleigh scattering correction, and biome type is required for the BRDF coupling correction. The LUT will also have the capacity to account for 3D adjacency effects, once such a parameterization is available for operational use. The Surface Reflectance IP is generated in twelve VIIRS spectral bands, listed in Table 1.

Table 1. The twelve VIIRS spectral bands in which Surface Reflectance will be computed.

Band Name	Center (microns)	Width (microns)	Nadir Resolution (m)
M1	.412	.020	750
M2	.445	.018	750
M3	.488	.020	750
M4	.555	.020	750
I1	.645	.050	375
M5	.672	.020	750
I2	.865	.039	375
M7	.865	.039	750
M8	1.24	.020	750
I3	1.61	.060	375
M10	1.61	.060	750
M11	2.25	.050	750

Raytheon

Four additional intermediate products in the VIIRS processing system must be generated from the Surface Reflectance IP: the Gridded Daily Surface Reflectance (GDSR) IP, Gridded Weekly Surface Reflectance (GWSR) IP, the Gridded Monthly Surface Reflectance (GMSR) IP, and the Monthly Non-Snow Reflectance (MNSR) IP.

The GDSR IP is a newly derived requirement for applying the MODIS heritage to albedo retrievals *[Y2398]*. It consists of a 16-day set of global gridded directional surface reflectances. These surface reflectances are remapped during offline processing from the pixel-level Surface Reflectance IP to a global 1-km grid using a methodology described in *[Y7051]*.

The GWSR IP is required by the Cloud Effective Particle Size and Cloud Optical Depth EDRs *[Y2393]*. It is a weekly or 8-day nadir-adjusted composite of the Surface Reflectance IP mapped to a global 1-km grid as described in *[Y7051]*. This product is generated in a moving window, updated daily.

The GMSR IP is required by the Surface Type EDR *[Y2402]*. It is a monthly nadir-adjusted composite of the Surface Reflectance IP mapped to a global 1-km grid as described in *[Y7051]*.

The MNSR IP is required by the Snow Cover/Depth EDR *[Y2401]*. It is a monthly nadir-adjusted composite of the Surface Reflectance IP for all pixels not categorized as snow, mapped to a global 1-km grid as described in *[Y7051]*. This product is generated in a moving window, updated daily.

3.0 ALGORITHM DESCRIPTION

3.1 PROCESSING OUTLINE

Figure 6 shows the operational flowchart for the Surface Reflectance IP. After determination of clear/cloudy and day/night for a given pixel, the heart of the process is the feeding of numerous inputs into a set of LUT interpolations, resulting in directional surface reflectances in the twelve VIIRS bands listed in Table 1. It is expected that after Phase II simulations and analyses, a number of the dimensions currently slated for the LUT will be moved into formulae and correction factors, with aerosols and solar/viewing geometry being retained as the primary LUT dimensions. The quality control (QC) flags generated from the Build SDR module and the cloud and aerosol inputs are fused into a single Land Quality Flag (LQF) structure that applies to the Surface Reflectance IP, the Surface Albedo EDR *[Y2398]*, the Vegetation Index EDR *[Y2400]*, the Surface Type EDR *[Y2402]*, the Soil Moisture EDR *[Y2387]*, and the Active Fires EDR *[Y3252]*. The LQF output is appended to the Surface Reflectance IP.

The Cloud Effective Particle Size and Cloud Optical Thickness EDRs are presently slated to be required for thin cirrus corrections. If waiting for these products introduces too much delay in operational processing time, thin cirrus handling will fall back to an empirically-based correction using VIIRS band M9 (1.38 µm). The final strategy will be detailed in Version 5 of this ATBD.
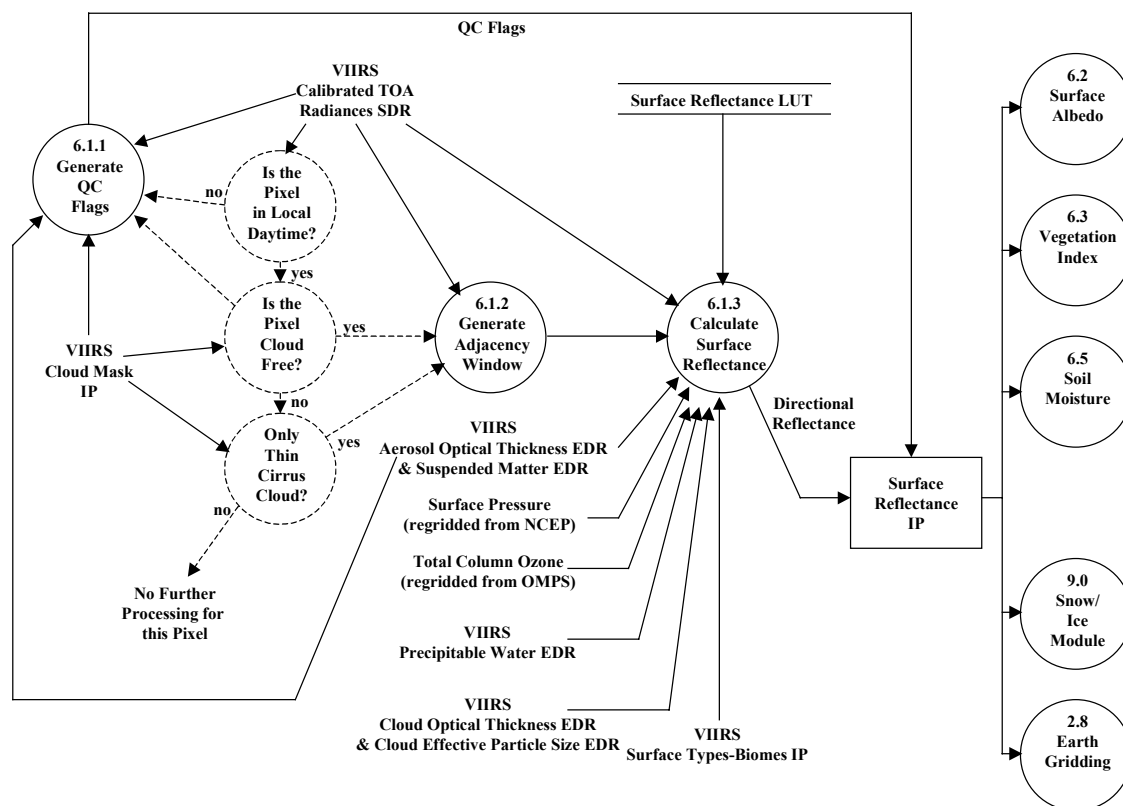
6.1 - SURFACE REFLECTANCE IP

Figure 6. Surface Reflectance IP processing architecture.

3.2   ALGORITHM INPUT

3.2.1 VIIRS Data

The Surface Reflectance IP algorithm employs the following VIIRS data:

- Aerosol Optical Thickness EDR *[Y2388]*

- Suspended Matter EDR *[Y2390]*

- Precipitable Water EDR *[Y3251]*

- Cloud Optical Thickness EDR (for thin cirrus correction, if viable) *[Y2393]*

- Cloud Effective Particle Size EDR (for thin cirrus correction, if viable) *[Y2393]*

- Calibrated TOA Radiances SDR (including radiances, geometry, geolocation, elevation, for bands M1, M2, M3, M4, I1, M5, I2, M7, M8, M9, M10, and M11) *[Y3261]*

- Cloud Mask IP (including cloud and land/water mask) *[Y2412]*

- Surface Types—Biomes IP *[Y2402]*

- Surface Reflectance LUT

3.2.2 Non-VIIRS Data

The Surface Reflectance IP algorithm employs the following non-VIIRS data:

- Surface Pressure from NCEP/Navy Operational Global Atmospheric Prediction System (NOGAPS) analyses

- Column Ozone from Ozone Mapping Profiling Suite (OMPS)

3.3   THEORETICAL DESCRIPTION—PHYSICS AND MATHEMATICAL BACKGROUND

The principal atmospheric components affecting TOA radiance in the range of 0.4-2.5 μm are shown in Figure 7. The related atmospheric processes can be grouped into two general classes: gaseous absorption and particle scattering. We define the true directional Surface Reflectance as

$$\rho_s(\lambda, \mu_0, \mu, \phi) = \frac{\pi L_s(\lambda, \mu_0, \mu, \phi)}{\mu_0 F_0(\lambda) T_0(\lambda, \mu_0, \phi)}, \tag{1}$$

where: λ is the wavelength in question (generally meaning the center wavelength of a given VIIRS band for the purposes of this document); μ_0 is the cosine of the solar zenith angle θ_0; μ is the cosine of the viewing zenith angle θ; ϕ is the relative azimuth angle; L_s is the reflected solar radiance emerging from the surface in the direction of μ; F_0 is the solar constant (flux) at the top of the atmosphere; and T_0 is the atmospheric transmission in the direction of μ_0. The factor π converts F_0 to an equivalent radiance parameter for standardization of ρ_s.

Raytheon

Ozone, Stratospheric Aerosols

20 Km

O_2, CO_2
Trace Gases

8 Km

Molecules (Rayleigh Scattering)

2-3 Km

H_2O, Tropospheric Aerosol

Ground Surface
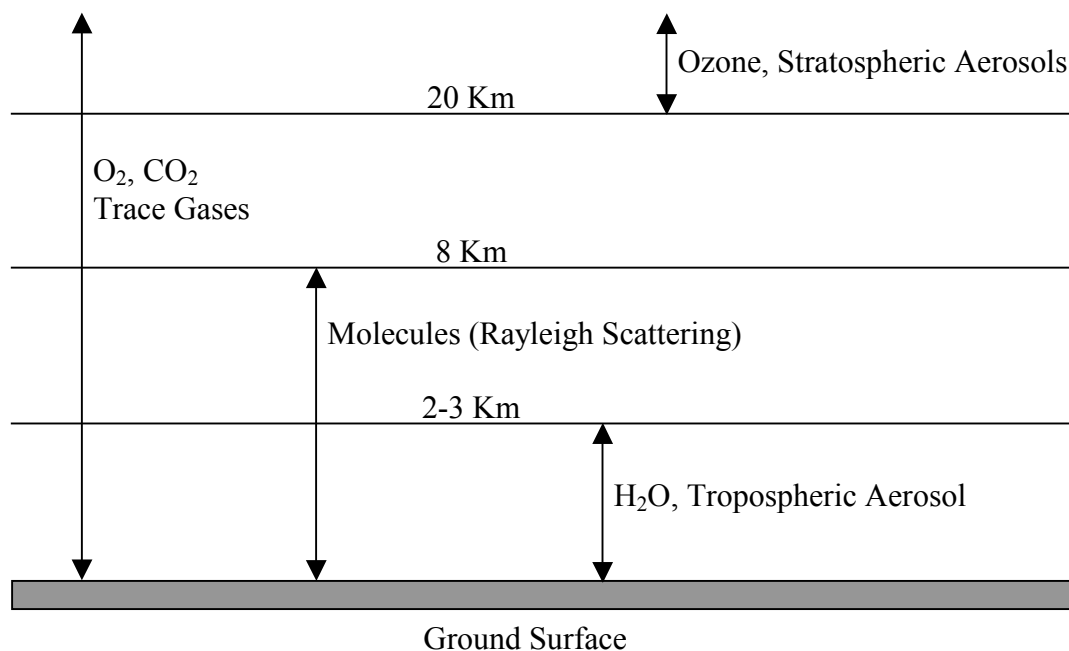
**Figure 7. The atmospheric components affecting the remote sensing signal
in the 0.4-2.5 µm range.**

If we assume a Lambertian surface, the radiance at the top of the atmosphere (TOA) measured by the VIIRS can be described as

$$L_{TOA}(\lambda,\mu_0,\mu,\phi) = \frac{T(\lambda,\mu,\phi)L_s(\lambda,\mu_0,\mu,\phi)}{[1-\rho_s(\lambda,\mu_0,\mu,\phi)S]} + L_{atm}(\lambda,\mu_0,\mu,\phi),$$ (2)

where T is the atmospheric transmission along the path μ, S is the reflectance of the atmosphere for isotropic light entering the base of the atmosphere, and L_{atm} is the path radiance. Both of the terms in the right-hand side of (2) include effects due to both absorption and scattering. The transmission of the surface reflected radiance is affected by extinction from both absorption and scattering, and the path radiance introduced by scattering is modified by atmospheric absorption. Substituting from (1) into (2), we obtain a relationship between the measured L_{TOA} and the sought-after quantity ρ_s:

$$L_{TOA}(\lambda,\mu_0,\mu,\phi) = \frac{T(\lambda,\mu,\phi)T(\lambda,\mu_0,\phi)\rho_s(\lambda,\mu_0,\mu,\phi)\mu_0 F_0(\lambda)}{\pi[1-\rho_s(\lambda,\mu_0,\mu,\phi)S]} + L_{atm}(\lambda,\mu_0,\mu,\phi).$$ (3)

It must be emphasized that (3) is only an approximation. In reality, the surface will not be Lambertian, and (3) will become considerably more complicated to account for anisotropy in both atmospheric and surface reflectance, in addition to the contributions of reflectance magnitude differences from surrounding pixels. Examples of mathematical accounting for these effects are provided in Vermote and Vermeulen (1999) and Lyapustin and Kaufman (2001). The Surface Reflectance lookup table (LUT), which will be operationally based on a given RT

model, is sufficiently generic that it can be separated from the exact formulation of surface and atmospheric bi-directional reflectance distribution function (BRDF) and adjacency effects. Consequently, mathematical details of these issues are left for a later version of this document, once the implementation strategy has been fully established. For the present, it is sufficient to note that the Surface Reflectance algorithm is essentially a multi-dimensional LUT based on the most accurate RT modeling available at the time of LUT generation. This allows a characterization of T_0, T, L_{atm}, and surface bi-directional and adjacency effects sufficient to map L_{TOA} to ρ_s.

3.3.1 LUT Dimensions

Table 2 summarizes the starting dimensions of the Surface Reflectance LUT. It must be stressed that this is only a starting point for Phase II refinement of the algorithm. Many of these dimensions will eventually be reduced to separate LUTs, empirical formulae, or correction factors to the output of the main LUT, as has been done for MODIS (Vermote and Vermeulen, 1999). Also, many of the entries suggested by Table 2 should not be populated, as they are not expected to be physically realizable. The suggested ranges and step sizes are also not necessarily the final values, but rather starting points that will be modified by the results of further sensitivity studies. It is expected that dimensions such as optical thickness will require much finer grids.

Table 2. Surface Reflectance lookup table (LUT) dimensions.

LAND LUT DIMENSIONS			
Index	Category	Dimension	Range
1	Spectral	VIIRS Band	[M1, M2, M3, M4, I1, M5, I2/M7, M8, I3/M10, M11]
2	Surface	Surface Directional Reflectance	[0.0, 0.05, 0.1, 0.2, … , 1.5]
3		BRDF (Surface Type)	[6 Biomes + Snow + Water + Soil]
4		Surface 3D Effects (Larger Spatial Average)	[0.0, 0.1, 0.2, 0.4, … , 1.4]
5	Atmosphere	Column Water Vapor (H2O) - mm	[0, 1.0, 2.0, 5.0, 10.0, 20.0, 40.0, 70.0, 100.0]
6		Column Ozone (O3) - Dobson units	[0, 130, 260, 390, 520, 650]
7		Atmospheric Profile	[Tropical, ML Sum, ML Win, SA Sum, SA Win, Arctic]
8		Tropospheric Aerosol Type	[Rur, Urb, Des, Mar, Ash, Smk]
9		Tropospheric Aerosol Optical Thickness	[0.0, 0.05, 0.1, 0.2, 0.4, 0.6, 0.8, 1.0, 1.5, 2.0]
10		Stratospheric Aerosol Type	[7 basic types in MODTRAN]
11		Cirrus Particle Size (Effective Radius) - µm	[0.0, 1.0, 5.0, 10.0, 20.0, 40.0, 80.0]
12		Cirrus Optical Thickness	[0.0, 0.05, 0.1, 0.2, 0.4, 0.7, 1.0]
13		Surface Pressure - hPa	[1050, 1000, 950, 900, 700, 500]
14	Geometry	Solar Zenith	[0.0, 10.0, 20.0, 30.0, 40.0, 50.0, 60.0, 70.0, 80.0]
15		View Zenith	[0.0, 10.0, 20.0, 30.0, 40.0, 50.0, 60.0, 70.0]
16		Relative Azimuth	[0.0, 22.5, 45.0, 67.5, 90.0, 112.5, 135.0, 157.5, 180.0]

3.3.1.1 Spectral Dimensions: VIIRS Band

The Surface Reflectance IP is delivered for the twelve bands listed in Table 1. These bands correspond to ten unique spectral ranges. From the standpoint of LUT utilization, differences in spatial resolution between imaging and moderate resolution bands are ignored. This strategy will be adjusted if further sensitivity studies indicate that adjacency effects do not scale sufficiently to guarantee meeting the performance specification for Surface Reflectance. Prior to actual measurements of the relative spectral response (RSR) in the VIIRS bands, the LUT is based on realistic simulations of the RSR as shown in Figure 4 and Figure 5. The current approach is to model the RSR as a modified Lorentzian:

Raytheon

$$RSR(\lambda) = \frac{1}{xE + 1} , \tag{4}$$

where E is an adjustable parameter that best characterizes the band shape and

$$x = \frac{|\lambda - \lambda_0|}{\Delta\lambda/2} , \tag{5}$$

with λ_0 representing the nominal band center and $\Delta\lambda$ signifying the nominal band width, defined by the full width half maximum (FWHM) of the RSR. This formulation has been determined from internal analyses by Raytheon SBRS to be quite accurate for representation of the MODIS bands, which are constructed from similar filter technology.

3.3.1.2 Surface Characterization Dimensions

The surface is characterized in the LUT by three dimensions: directional reflectance, BRDF, and adjacency effects. The directional reflectance is the parameter being retrieved, and is therefore the target of the interpolation across all other dimensions. It is possible for the directional reflectance to be higher than 1. Setting the reflectance magnitude for a given path is easily implemented in any RT model. The contextual treatment of BRDF and adjacency effects is much more complicated. Until recently, this capability did not exist in MODTRAN or DISORT. The latest versions at this writing, however, allow for a treatment of both effects (BRDF in both MODTRAN and DISORT, adjacency effects in MODTRAN only). 6S has had this capability for a longer period of time, implemented in a slightly different fashion. As RT models become more advanced, the treatment of these effects is expected to become more accurate. The present strategy for the VIIRS Surface Reflectance algorithm is to establish placeholder dimensions and provide detail on the exact nature of the RT modeling in a future version of this document. In brief, the dimension for atmospheric/BRDF coupling will consist of several standard BRDF shapes, beginning with the Surface Types—Biomes IP *[Y2402]*, and adding basic models for water, snow, and bare soil or sand. These extra types may even be fused into the production of the Surface Types—Biomes IP. The dimension for adjacency effects is a measure of the brightness of surrounding pixels, computed to first order from the TOA radiances in the surrounding pixels relative to the TOA radiance in the central pixel for which Surface Reflectance is being retrieved.

3.3.1.3 Gaseous Absorption Dimensions

The primary gaseous absorbers affecting the variability of TOA radiances in the VIIRS reflective bands are water vapor (H_2O) and ozone (O_3), which both exhibit substantial variability across the globe, throughout the year, and as a function of height in the atmosphere. Carbon dioxide (CO_2), oxygen (O_2), methane (CH_4), nitrous oxide (N_2O), and carbon monoxide (CO), by contrast, are either fairly well-mixed or do not have prominent spectral absorption features within the limits of the VIIRS spectral bands, as seen in Figure 4 and Figure 5. The most prominent O_2 feature is the A-band, which is located near VIIRS band M6; this band is not used in Surface Reflectance retrievals. The only significant CO_2 feature in the VIIRS reflective bands is within bands I3 and M10, however this feature is not strong enough to have a significant impact on TOA radiances,

as shown in Figure 8, which is based on MODTRAN 4.0 simulations. These simulations are described in more detail in Section 3.4.1.3. Sensitivity to absorption by H_2O and O_3 for the VIIRS bands is presented in Sections 3.4.2.3 and 3.4.2.4. Each of these gases has a corresponding dimension in the Surface Reflectance LUT. Operationally, the inputs for these two parameters will exist in the form of the VIIRS Precipitable Water EDR *[Y3251]* and the OMPS total column ozone product, respectively.
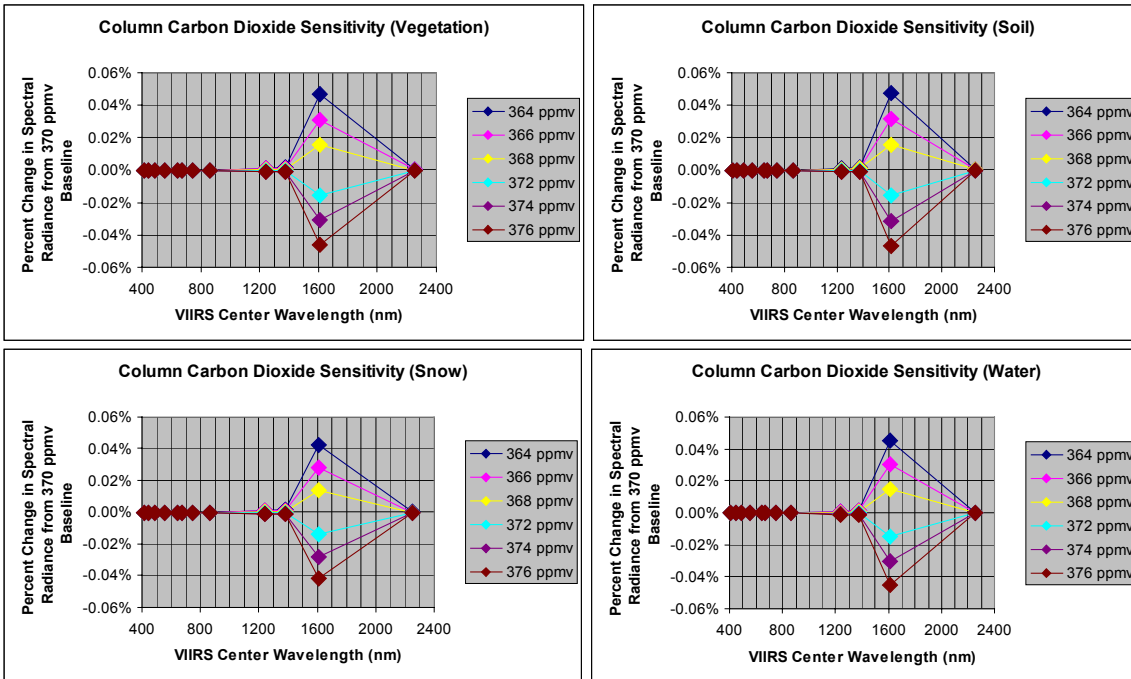
Figure 8. Sensitivity of TOA radiance to column carbon dioxide in the VIIRS reflective bands.

3.3.1.4 Aerosol Dimensions

As the sensitivity studies documented in Sections 3.4.2.6, 3.4.2.7, and 3.4.2.8 indicate, aerosols are the largest atmospheric contributor to variability and uncertainty in the retrieval of Surface Reflectance. Three dimensions are devoted to aerosols in the Surface Reflectance LUT: tropospheric aerosol type, tropospheric aerosol optical thickness, and stratospheric aerosol type. The tropospheric aerosol dimensions will originate operationally in the VIIRS Aerosol Optical Thickness *[Y2398]* and Suspended Matter *[Y2390]* EDRs. The aerosol optical thickness range in the LUT has been set to the specified measurement range for the VIIRS Aerosol Optical Thickness EDR. For retrievals with an aerosol optical thickness higher than a certain threshold (baselined at 0.5 for the present), the Land Quality Flag (LQF) output will indicate significant aerosol obscuration. A baseline set of aerosol types has been listed in Table 2, but the list will evolve in future versions of this document, concurrent with refined mapping between those aerosol types that are reliably modeled in current RT models and the output of the Suspended Matter EDR.

Raytheon

Figure 9 shows the optical properties of typical stratospheric aerosol, maritime aerosol, desertic aerosol, biomass burning aerosol, continental aerosol, and urban aerosol. Stratospheric, maritime, desertic, and continental aerosol exhibit a high single scattering albedo in the visible/near infrared (VNIR) and short wave infrared (SWIR) portion of the spectrum; urban aerosol has the lowest single scattering albedo. The six types of aerosol shown have similar asymmetry in the VNIR wavelengths, but differences in asymmetry arise when the wavelength is greater than 1.5 µm. All the aerosol types shown have similar phase functions for scattering.
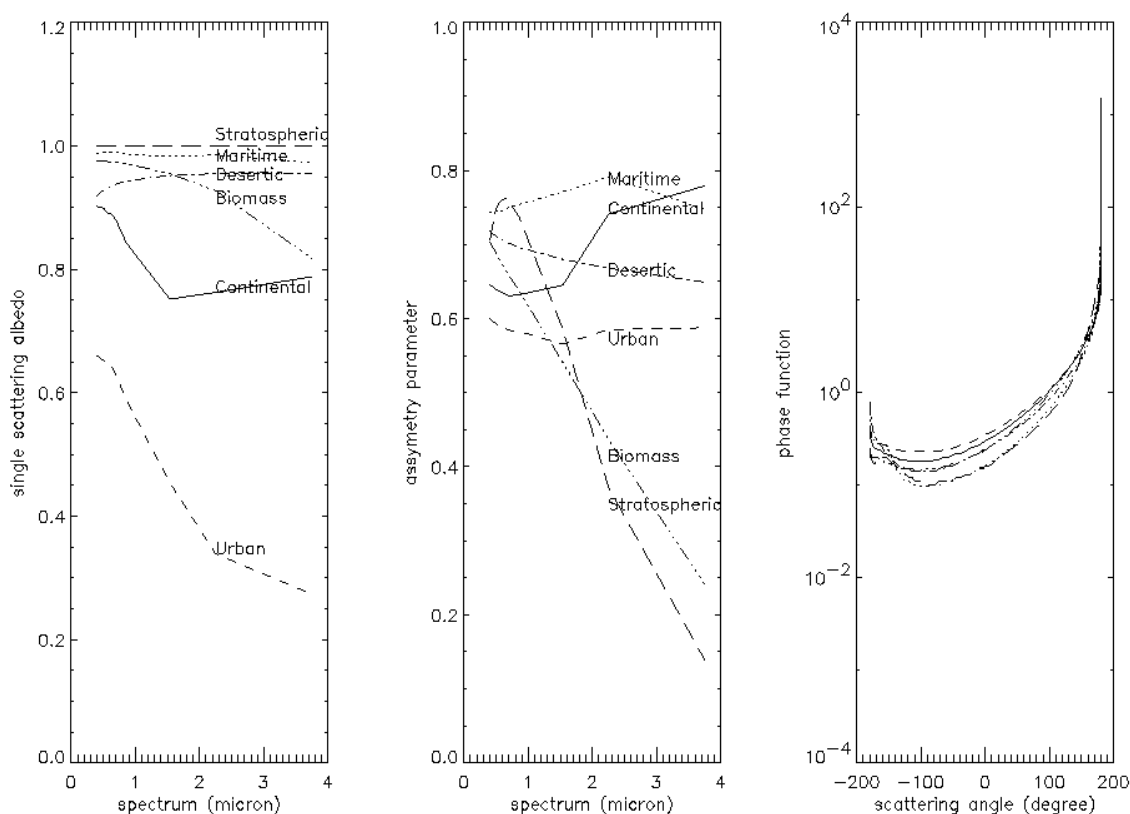
Figure 9. Scattering properties (single scattering albedo, asymmetry parameter, phase function) of different aerosol types.

The LUT dimension for Stratospheric aerosol type refers to additional aerosol effects from volcanic eruptions. Where such aerosol is detected by the Suspended Matter EDR, the Land Quality Flag output will indicate stratospheric aerosol obscuration. The Surface Reflectance IP and downstream products are not guaranteed to meet performance specifications for accuracy, precision, and uncertainty in the presence of stratospheric aerosol beyond the "background" type simulated by the RT model used to generate the LUT.

3.3.1.5 Cirrus Correction Dimensions

In the presence of thin cirrus (presently defined to possess optical thickness ranging up to 1), the Surface Reflectance IP and downstream products are generated, with an associated flag in the Land Quality Flag output. The baseline approach is to use the VIIRS Cloud Effective Particle

Size and Cloud Optical Thickness EDRs *[Y2393]* as the inputs for the two cirrus parameter dimensions listed in Table 2. These will be used to interpolate against the cirrus particle size and optical thickness simulated in the RT model. Pixels for which the retrieved cirrus optical thickness exceeds a TBD threshold value will not be guaranteed to meet the performance specifications for accuracy, precision, and uncertainty in Surface Reflectance or its downstream products. In case waiting for the Cloud EDRs is not operationally viable, a secondary approach for correcting thin cirrus contamination will be to use VIIRS band M9 (1.38 μm) in an empirically based fashion to correct the reflectances in the bands for which Surface Reflectance is to be retrieved. Tradeoffs between this approach and the direct use of VIIRS cloud optical properties products will be presented in future versions of this document.

3.3.1.6 Molecular Scattering Dimension

In the shorter VIIRS wavelengths, Rayleigh scattering from molecules has a significant effect on the radiance reaching the top of the atmosphere. The two largest contributors to Rayleigh scattering are the two most abundant gases in the atmosphere—oxygen and nitrogen. These two gases are well-mixed, and so the primary source of variability in Rayleigh scattering is the latitudinal, seasonal, topographic, and synaptic variability in atmospheric pressure, particularly near the surface. Consequently, the Surface Reflectance LUT must have a dimension allowing adjustment to Rayleigh scattering effects. The baseline parameter for this dimension is surface pressure, to be obtained operationally from National Centers for Environmental Prediction (NCEP) analyses.

3.3.1.7 Angular Dimensions

The last three dimensions in the LUT correspond to the three angles that specify the solar and viewing geometry for a given pixel: solar zenith, view zenith, and relative azimuth. The signal at the top of the atmosphere varies dramatically depending on these three parameters; the step size for each will need to be fine enough to ensure optimal interpolation.

3.4 ALGORITHM SENSITIVITY STUDIES

The performance of the Surface Reflectance algorithm is limited by several key error sources, including interpolation within the LUT, sensor effects, atmospheric effects, and coupling of the atmosphere and surface BRDF. The atmospheric effects include aerosol and Rayleigh scattering, gaseous absorption, and thermodynamic conditions. The majority of the error for the VIIRS Surface Reflectance IP comes from uncertainties in the aerosol properties. The primary sensor effect is calibration error. Because VIIRS has been driven to an extremely low-noise design by the requirements for Ocean Color and Sea Surface Temperature retrievals, sensor noise is a minor error term for Surface Reflectance.

3.4.1 Performance Metrics and Description of Simulations

Several error sources have been identified and investigated in the development of the VIIRS Surface Reflectance algorithm, and each will be detailed in the following subsections:

1) LUT Interpolation

2) BRDF Coupling

3) Column Water Vapor

4) Column Ozone

5) Atmospheric Profile

6) Tropospheric Aerosol Optical Thickness

7) Tropospheric Aerosol Type

8) Stratospheric Aerosol Type

9) Cirrus Particle Size and Optical Thickness

10) Surface Pressure (Rayleigh Scattering)

11) Sensor Noise

12) Sensor Calibration

Other errors exist, however most are negligible in comparison with a few key sources listed above, notably aerosols and calibration. Sensor modulation transfer function (MTF) errors can be significant over heterogeneous surfaces, however these are difficult to quantify on a global basis, and they will be deferred to the ATBDs for the downstream products such as the Vegetation Index EDR *[Y2400]*. All of the sensitivity studies presented here should be considered works in progress; the advent of VIIRS-like spectral and radiometric capability with MODIS is just now beginning to reveal the true performance characteristics of modern atmospheric correction algorithms, and the estimates presented here will be refined as understanding of both the geophysics and the instrument characterization evolve. Some error sources, such as stratospheric aerosol or cirrus properties, have received comparatively little attention to date. Others, such as sensor noise and aerosol optical thickness, have been investigated more thoroughly.

There are no explicit quality requirements on the Surface Reflectance IP in the VIIRS SRD. We have, however, derived performance estimates for surface reflectance retrievals to assist in the error budgeting for the VIIRS EDRs requiring this product as an input. Following the SRD, we have estimated performance in terms of three metrics: accuracy, precision, and uncertainty.

Consider a single true value T of a product at the pixel level. A satellite-borne sensor will produce data that can be transformed through a retrieval algorithm into an estimate X_i of T, where $i = 1, N$ indicates that any arbitrary number N of such estimates can be made. Various error sources along the retrieval pipeline between the true value T and the measured value X_i will cause X_i to deviate from T. The accuracy is defined as

$$A = |\mu - T| \qquad\qquad\qquad\qquad (6)$$

where $\mu = \dfrac{1}{N}\sum_{i=1}^{N} X_i$. The accuracy can also be referred to as a bias and is a direct comparison between the measurement X_i and the true value T.

For a single value of truth, the precision is defined as the standard deviation of the measurement:

$$P = \left[\frac{1}{N-1}\sum_{i=1}^{N}(X_i - \mu)^2\right]^{\frac{1}{2}} \tag{7}$$

While mathematically the calculation of the precision as defined is independent of the true value T, it must be remembered that (7) is computed for a specific true value T, and the choice of T will affect the value of P.

The uncertainty is defined as:

$$U = \left[\frac{1}{N-1}\sum_{i=1}^{N}(X_i - T)^2\right]^{\frac{1}{2}} \tag{8}$$

The uncertainty is therefore akin to a root mean square (RMS) error between the estimated X_i and the true value T.

For variable truth data sets, the practical implementation of the definition on accuracy, precision, and uncertainty is to bin the possible values of T into ranges that are large enough to provide a statistically significant number of test points but small enough to facilitate useful figures of merit.

The definitions of accuracy, precision and uncertainty in this case are:

$$A = \left[\mu - \mu_T\right], \tag{9}$$

$$U = \left[\frac{1}{N-1}\sum_{i=1}^{N}(X_i - T_i)^2\right]^{\frac{1}{2}}, \tag{10}$$

$$\boldsymbol{P^1} = \left(\boldsymbol{U^2} - \boldsymbol{A^2}\right)^{1/2}, \tag{11}$$

where μ_T is the mean of the true values in the statistical ensemble and T_i is the true value corresponding to the measurement X_i.

The performance results discussed in the following sections emerged from three main sets of simulations:

1) Phase I scene simulations using Terrain Categorization (TERCAT) scenes based on Landsat Thematic Mapper (TM) imagery

Raytheon

2) Phase I "stick modeling" simulations that deal with the radiative transfer for a single linear path through the atmosphere

3) Phase II stick modeling focused more exclusively on each individual error source, particularly those associated with the atmosphere.

In all three cases, MODTRAN was the primary forward model used. MODTRAN 3.7 (Kneizys *et al.*, 1996) was the basis for the Phase I efforts. MODTRAN 4.0 (Berk *et al.*, 1999) was used for Phase II simulations.

3.4.1.1 IPO-Supplied TERCAT Scenes

A limited degree of end-to-end testing was conducted using IPO-supplied TERCAT scenes. In particular, extracts from three scenes were investigated by the land team: Amazon, Olympic Peninsula, and Bangladesh. Results from the Amazon scene are deferred to the Vegetation Index ATBD *[Y2400]*. The other two scenes are shown in Figure 10 and Figure 11.
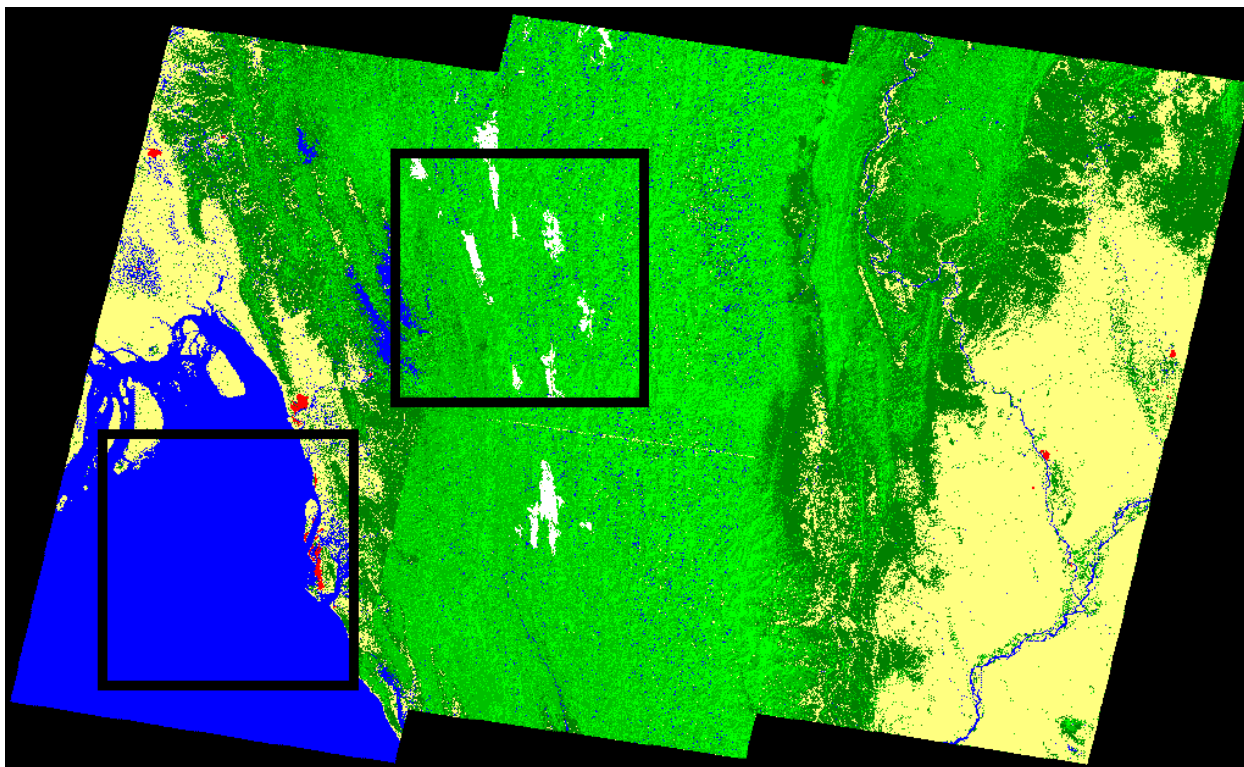
Figure 10. Classification map of the Bangladesh scene. Mostly forest (green), bare soil (sandy color), and water (blue). Clouds are indicated in white. Boxes indicate subscenes for which sensitivity studies were conducted.
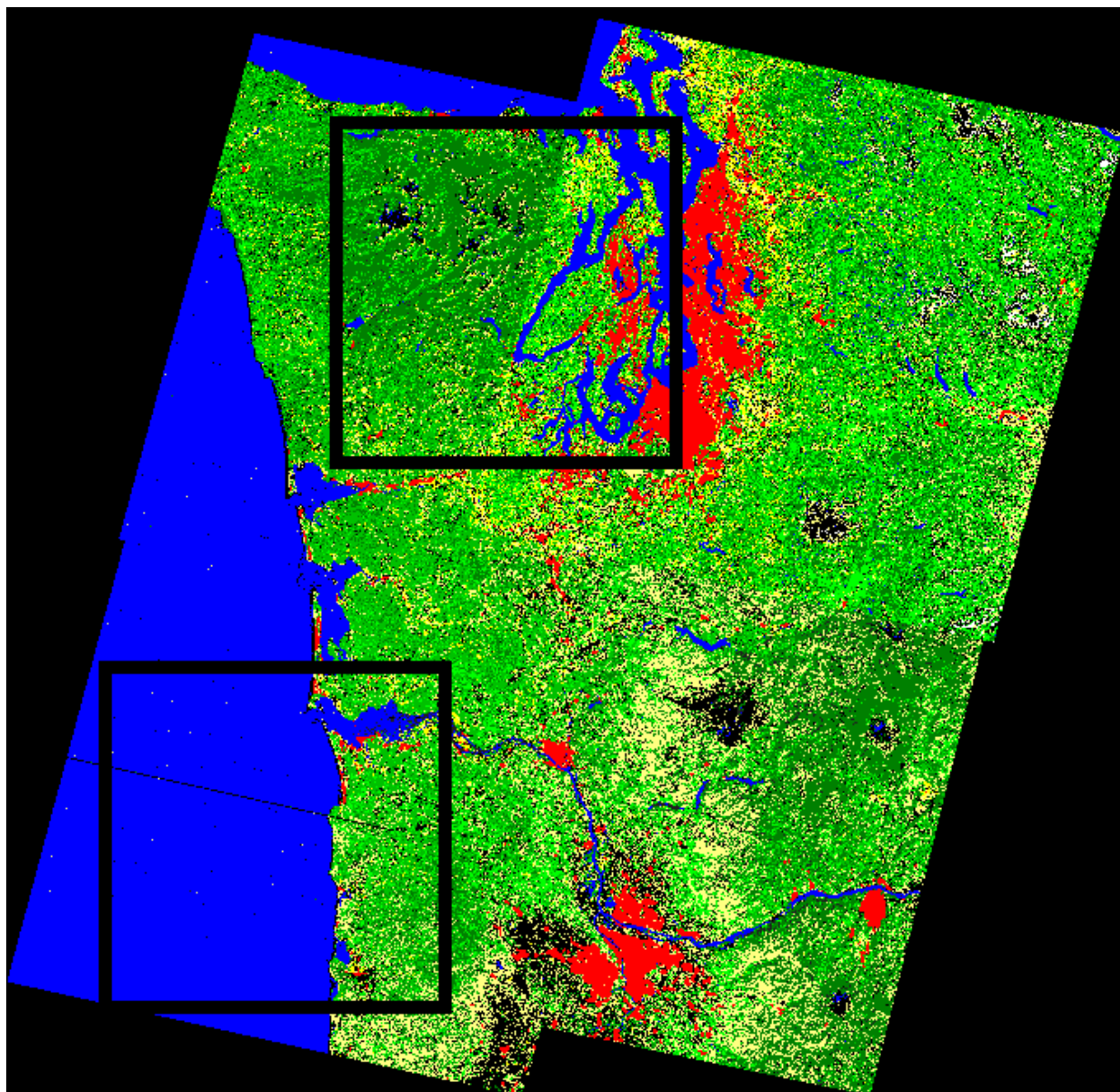
Figure 11. Classification map of the Olympic Peninsula scene. Very heterogeneous, with vegetation (green), water (blue), urban (red), and small amount of snow (white). Boxes indicate subscenes for which sensitivity studies were conducted.

The TERCAT classification maps at 50-m resolution were converted to VIIRS surface spectral reflectances via the NPOESS spectral library, which includes data originating from the ASTER spectral library (http://speclib.jpl.nasa.gov/). These reflectances were used as inputs to forward modeling using MODTRAN 3.7. The surface reflectances and the independently supplied surface temperature map were aggregated to produce "truth" for surface reflectance, albedo, vegetation indices, and surface temperature. The dominant class in an aggregated VIIRS-sized pixel was chosen as truth for surface type.

For atmospheric effects, the MODTRAN midlatitude summer profile was used. Rural aerosols were applied, with aerosol optical thickness being spatially discretized into several image-wide bands ranging from approximately 0.2 to 0.8. Realistic viewing and solar geometry were applied using the Science Data Processing (SDP) Toolkit as though the data were obtained from a segment of a VIIRS swath.

The result of the forward modeling was a 50-m resolution map of top of atmosphere (TOA) radiances. These TOA radiances were spectrally integrated using a tophat response function, creating 16 VIIRS spectral bands for use by EDR algorithms. MTF blurring, sensor noise, and calibration errors were sequentially simulated as described in Hucks (1998). The output of this process was a simulated set of measured TOA radiances.

Since the simulations were conducted midway through Phase I, the spectral bands simulated for the TERCAT scenes have a different nomenclature than the current indexing indicated in Table 1. Table 3 shows the mapping between the old and new band names.

Table 3. Mapping between old (Phase I) and new (Phase II) VIIRS spectral band names.

New Band Name	Center (microns)	Width (microns)	Old Band Name
M1	.412	.020	Chlor2
M2	.445	.018	Viirs2
M3	.488	.020	Chlor8
M4	.555	.020	Viirs4
I1	.645	.050	Viirs5
M6	.746	.015	Oc2
I2	.865	.039	Viirs6
M8	1.24	.020	Cloud1
I3	1.61	.060	Viirs8
M11	2.25	.050	Viirs9

The retrieval pipeline started with cloud masking, followed by aerosol retrievals. Finally, various surface products were retrieved and compared with the truth. For Land EDRs and intermediate products (IPs), this included Surface Reflectance, Vegetation Index, Surface Albedo, and Surface Type.

Since the TERCAT scenes provided only a limited range of atmospheric and geometric conditions, the results of this processing were primarily used to confirm the MTF and band to band registration (BBR) errors suggested from the Landsat TM simulations. The magnitude of the effects was similar between data sets for both error sources. MTF and BBR errors are discussed in detail in the Vegetation Index ATBD *[Y2400]*; they will not be considered in this document. Some results of aerosol, gaseous absorption, and temperature/pressure sensitivities presented here were derived from the TERCAT scene simulations.

3.4.1.2   Phase I Stick Modeling

The majority of the performance stratification work presented in the Phase I version of the VIIRS Verification and Validation Plan is based upon a large ensemble of "stick model simulations"—RT and sensor modeling for a single linear path through the atmosphere without consideration of 3D effects. The dimensions of this data set are summarized in Table 4.

Table 4. Summary of dimensions for Phase I Land EDR "stick modeling" data set.

Parameter	# Different Values	Range
Surface Type	10	Coniferous forest, deciduous forest, shrub, grass, crops, urban, snow, bare soil, desert sand, water
Solar Zenith	8	0-70 degrees
Scan Angle	7	0-60 degrees
Relative Azimuth	5	0-180 degrees
Aerosol Type	4	Urban, rural, desert, LOWTRAN maritime
Aerosol Optical Thickness	5	0.1-0.5

Spectral reflectance data were derived from the ASTER library. All forward modeling was conducted using MODTRAN 3.7, with a midlatitude summer profile. The output of each stick model simulation consisted of a true broadband surface albedo, true TOA reflectances in nine spectral bands, and true surface reflectances in nine spectral bands (all the wavelengths listed in Table 1 except for M5). The true reflectances were used to generate true values of NDVI and EVI at both top of canopy (TOC) and top of atmosphere (TOA).

3.4.1.3   Phase II Stick Modeling

Stick modeling in Phase II employed MODTRAN 4.0. More focus was placed on individual atmospheric error sources, to provide initial guidance on the design of the Surface Reflectance LUT. The parameters used for each set of runs will be described in each of the relevant subsections under Section 3.4.2. In all cases, a solar zenith of 20º, a view zenith of 30º, and a relative azimuth of 0º (forward scattering) were used.

3.4.2   Individual Error Sources

3.4.2.1   LUT Interpolation

Since the Surface Reflectance algorithm is a finite LUT, calculations of surface reflectance will incur errors from interpolation between LUT elements. Figure 12 shows a rudimentary estimate of the effects for several VIIRS bands, based on Phase I simulations with the Olympic Peninsula TERCAT scene. In general, the errors are quite small, however this is by no means a thorough assessment. The dimensions investigated in Phase I were limited and their respective ranges were not comprehensive. A more rigorous evaluation of this error source, which forms much of the basis for the very structure of the LUT, will be carried out in Phase II and summarized in Version 5 of this document.

Raytheon
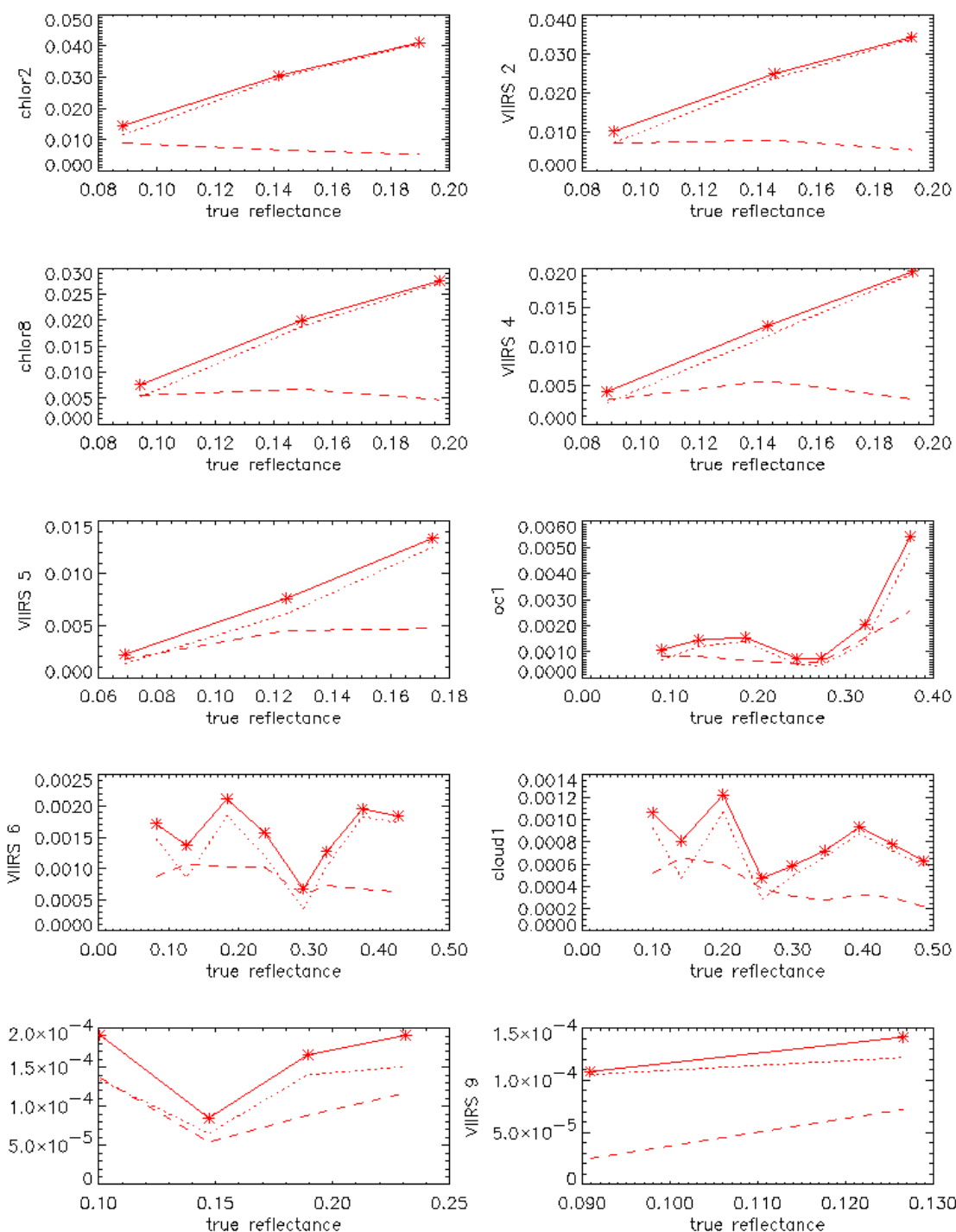
Figure 12. Interpolation error as a function of reflectance for several VIIRS bands, based on Phase I simulations with the Olympic TERCAT scene. See Table 3 for a mapping of band names in this figure to the new band names.

3.4.2.2   BRDF/Atmospheric Coupling

For a Lambertian surface, i.e., a surface that scatters light isotropically, radiative interactions between the atmosphere and its background can be treated straightforwardly in a geometric (doubling) manner, but an anisotropic land surface leads to very complicated coupling between the atmosphere and the background surface. Failure to account for surface BRDF effects in atmospheric correction can consequently lead to significant errors in surface reflectance retrieval (Lee and Kaufman, 1986).

Several numerical radiative transfer models that make use of matrix operators, Gauss-Seidel, successive orders of scattering, and discrete ordinates methods have been developed for solving the coupling between the atmosphere and its lower boundary (Vermote *et al.,* 1997). Lyapustin (1999) uses spherical harmonics to model the coupling of the atmosphere and the non-Lambertian land surface. In the Phase I algorithm development effort, we employed the approach used in 6S, i.e., the Successive Orders of Scattering Method, to solve the radiative transfer equation in the atmosphere (Vermote *et al.,* 1997). This provided a basis for estimating the errors introduced by atmospheric coupling to surface BRDF. In the following, we analyze the effects of a non-Lambertian surface on the retrieval of directional reflectance of land surfaces from VIIRS measurements. Only a conifer forest background was considered here, with several discrete values of aerosol optical thickness. A hybrid geometric-optical and radiative transfer model developed for discontinuous plant canopies (Ni *et al.,* 1998) was used to generate the surface BRDF. The TOA directional reflectances in the principal plane and the cross-principal plane with different aerosol optical thicknesses for bands Viirs4, Viirs5, and Viirs6 (555 nm, 645 nm, and 865 nm, respectively; see Table 3 for a mapping of band names in this discussion to the new band names) are shown in Figure 13 and Figure 14. A continental aerosol model and midlatitude summer atmosphere were used in the simulations. The surface BRDF values are also included in Figure 13 and Figure 14 for comparison. Several observations can be made:

- The directional reflectances in the principal plane (the starred line in the plots) exhibit a bowl shape with a strong hotspot for backward scattering. Scattering makes this bowl shape much smoother than it would be without an aerosol-laden atmosphere.

- In the principal plane, for the visible part of the spectrum (bands Viirs4 and Viirs5), the TOA directional reflectances lead to overestimation of the surface BRDF, due to the predominance of Rayleigh scattering as opposed to absorption. This overestimation becomes larger with increased viewing zenith angles, and it is stronger for forward scattering than for backward scattering, due to the strong forward scattering peak of aerosol particles. This effect increases in strength with the increase of solar and viewing zenith angles, due to increased path length.

- In the near-infrared wavelengths (band Viirs6), the algorithm overestimates the surface reflectance in the forward scattering direction, due to stronger forward scattering of aerosols and lower surface reflectances, leading to a predominance of scattering over absorption. Meanwhile, the algorithm underestimates the surface reflectances in the backward scattering direction, due to larger surface reflectance and the predominance of absorption over scattering.

- In the cross-principal plane, in bands Viirs4 and Viirs5, atmospheric scattering causes an overestimation of the surface reflectances at solar zenith angles of 30° and 60°. In band Viirs6, at a solar zenith angle of 30°, atmospheric scattering has virtually no effect on the

Raytheon

retrieved surface reflectance, because scattering and absorption effect counterbalance each other. At a solar zenith angle of 60°, atmospheric scattering again begins to dominate.

- A comparison of Figure 13 and Figure 14 indicates that atmospheric effects on surface reflectance retrievals intensify with an increase in path length.

A BRDF-based atmospheric correction equivalent to the MODIS approach was used to retrieve the surface reflectance from the TOA measurements simulated in Figure 13 and Figure 14. The resulting comparison of the retrieved and true surface bidirectional reflectances is shown in Figure 15 and Figure 16. Even when correcting for surface BRDF effects, the performance degrades for higher values of aerosol optical thickness.
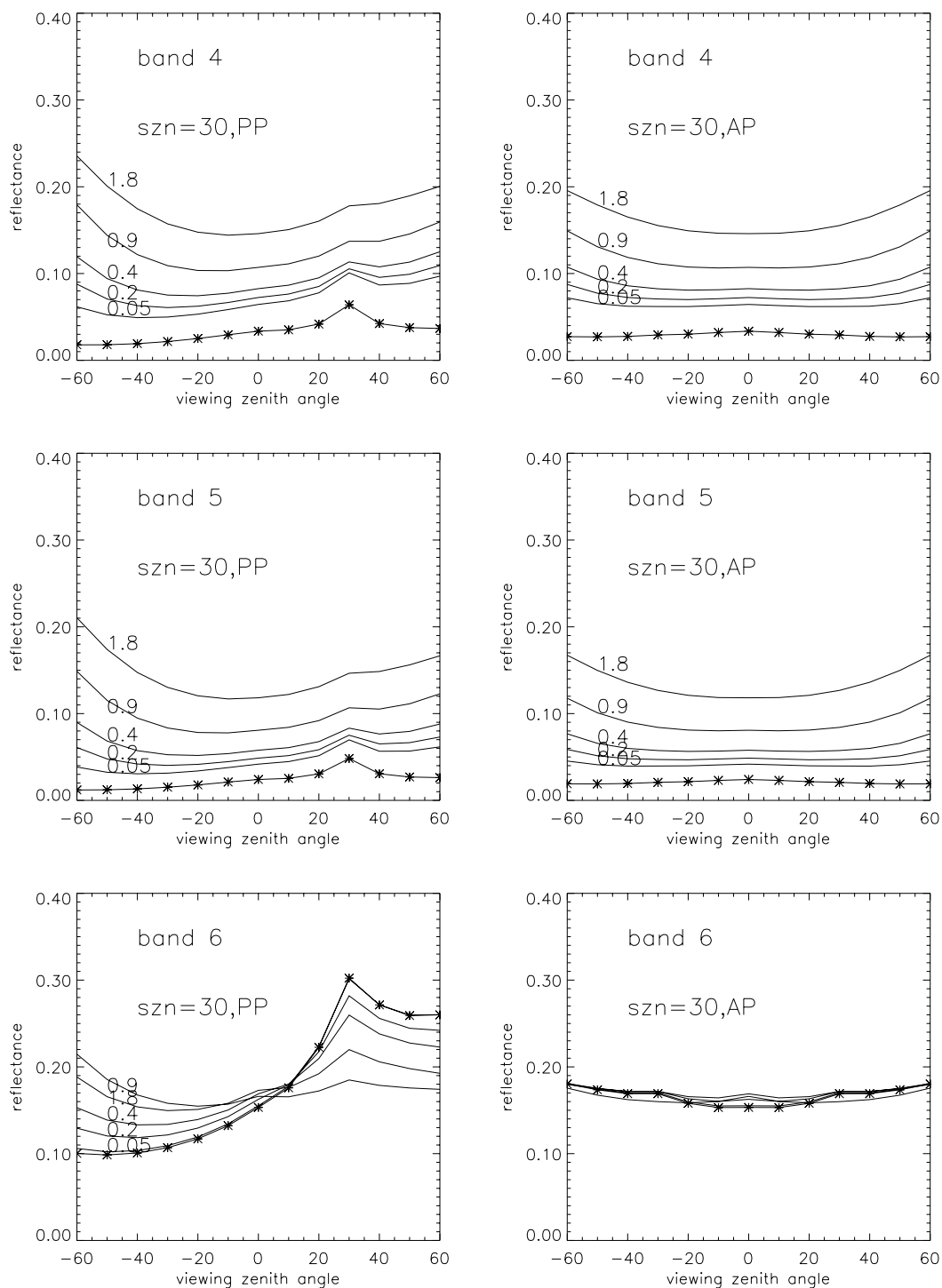
Figure 13. Comparison between surface (with *) and TOA (without *) directional reflectance from 6S, in the principal plane (left) and the cross-principal plane (right) for bands Viirs4, Viirs5, and Viirs6 at 30 º solar zenith with varying aerosol optical thickness. See Table 3 for a mapping of band names in this figure to the new band names.
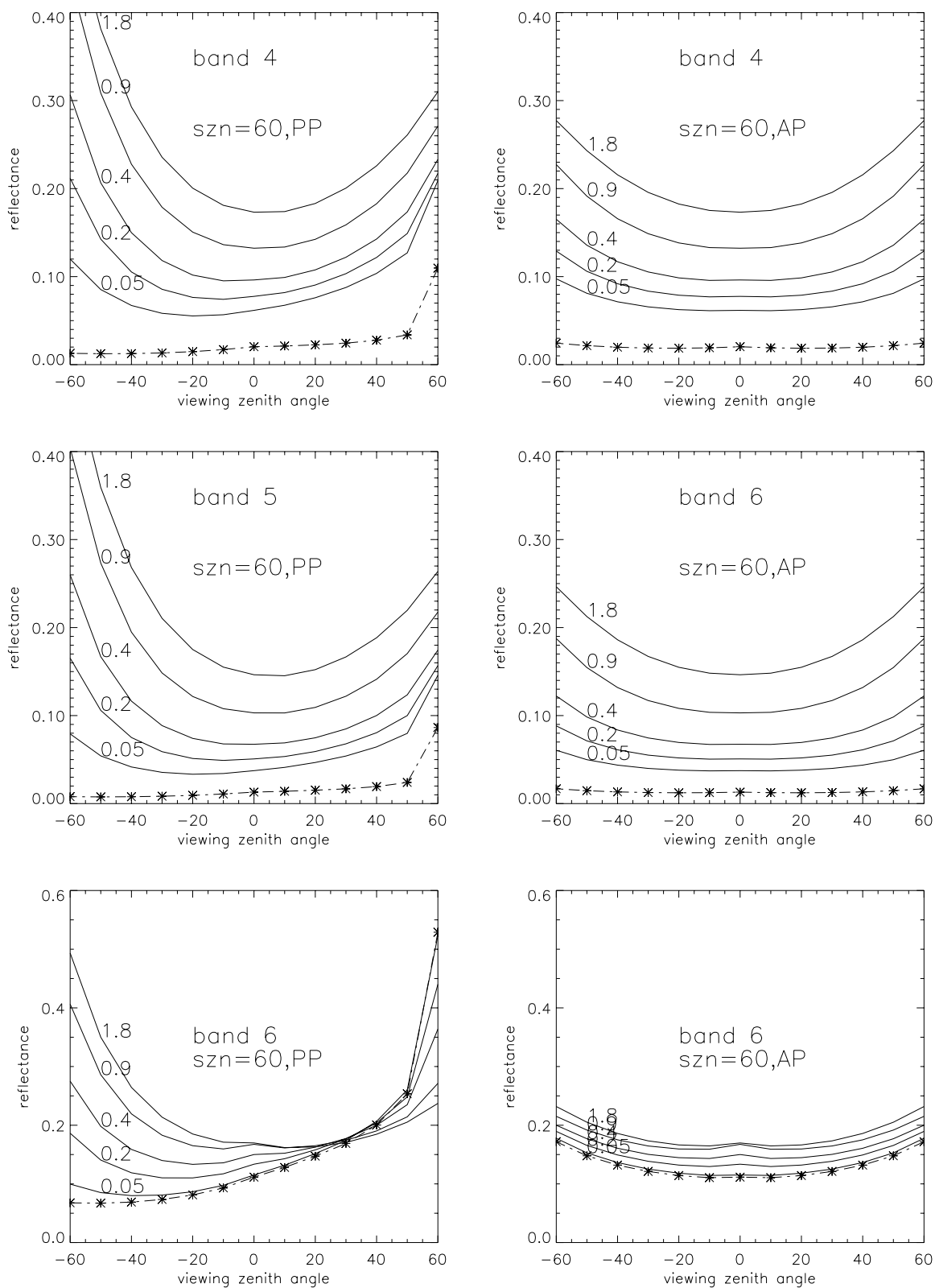
Figure 14. Comparison between surface (with *) and TOA (without *) directional reflectance from 6S, in the principal plane (left) and the cross-principal plane (right) for bands Viirs4, Viirs5, and Viirs6 at 60 º solar zenith with varying aerosol optical thickness.
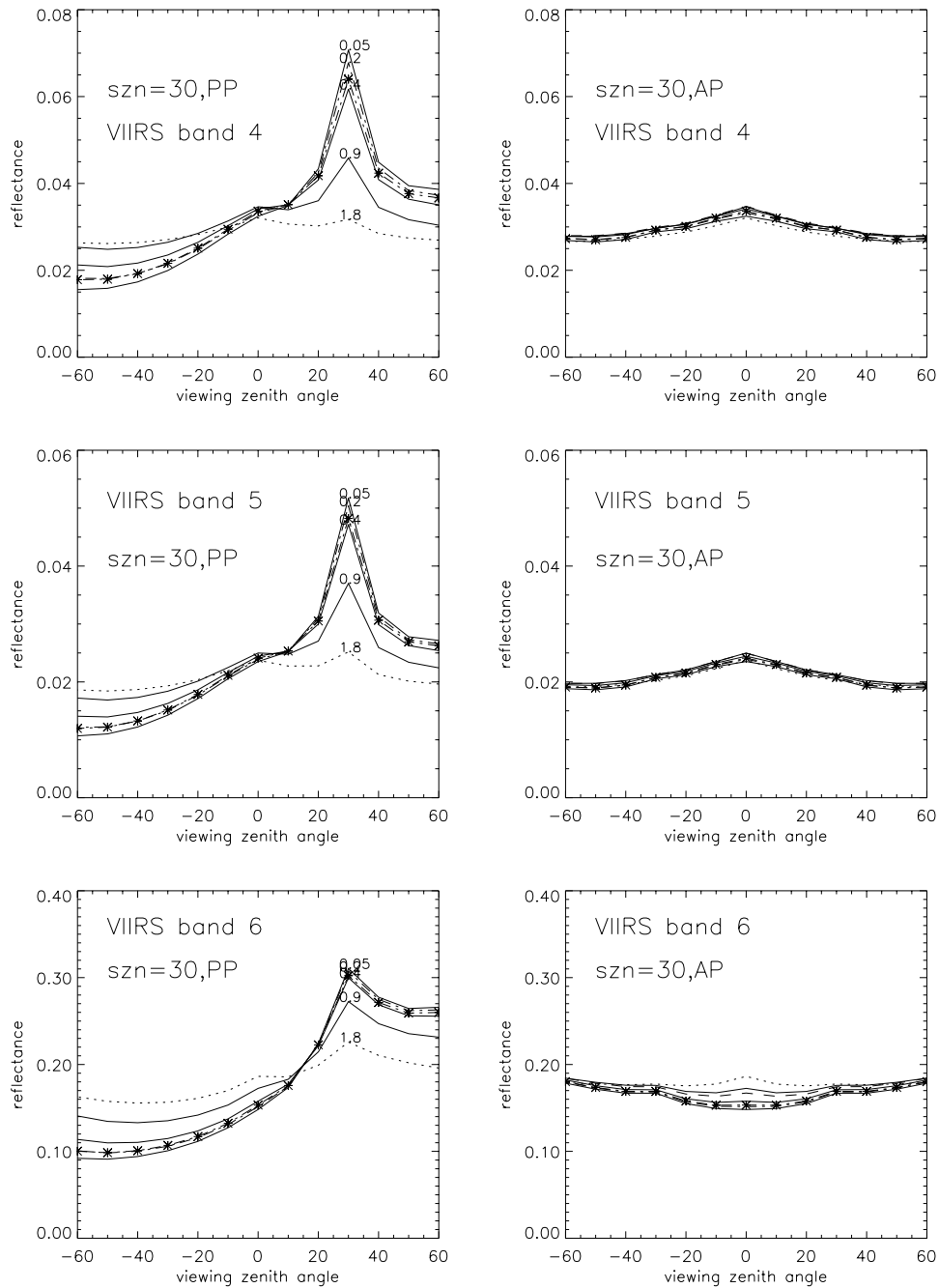
Figure 15. True (with *) and retrieved (without *) surface reflectances from 6S, using non-Lambertian-based atmospheric correction, in the principal (left) and cross-principal (right) planes, for bands Viirs4,Viirs5, and Viirs6 at a solar zenith of 30 º, for varying aerosol optical thickness. See Table 3 for a mapping of band names in this figure to the new band names.

Figure 16. True (with *) and retrieved (without *) surface reflectances from 6S, using non-Lambertian-based atmospheric correction, in the principal (left) and cross-principal (right) planes, for bands Viirs4,Viirs5, and Viirs6 at a solar zenith of 60 º, for varying aerosol optical thickness. See Table 3 for a mapping of band names in this figure to the new band names.
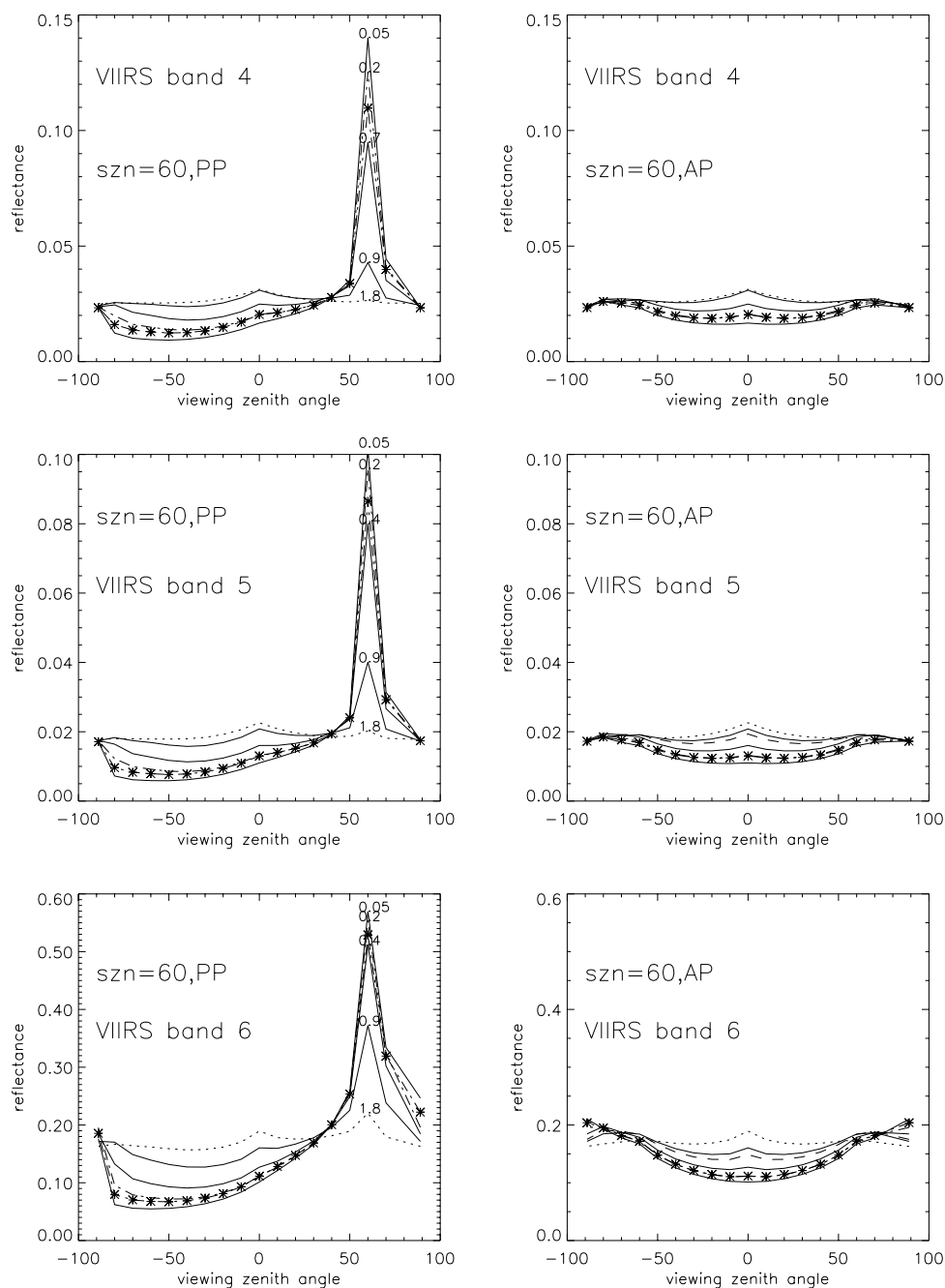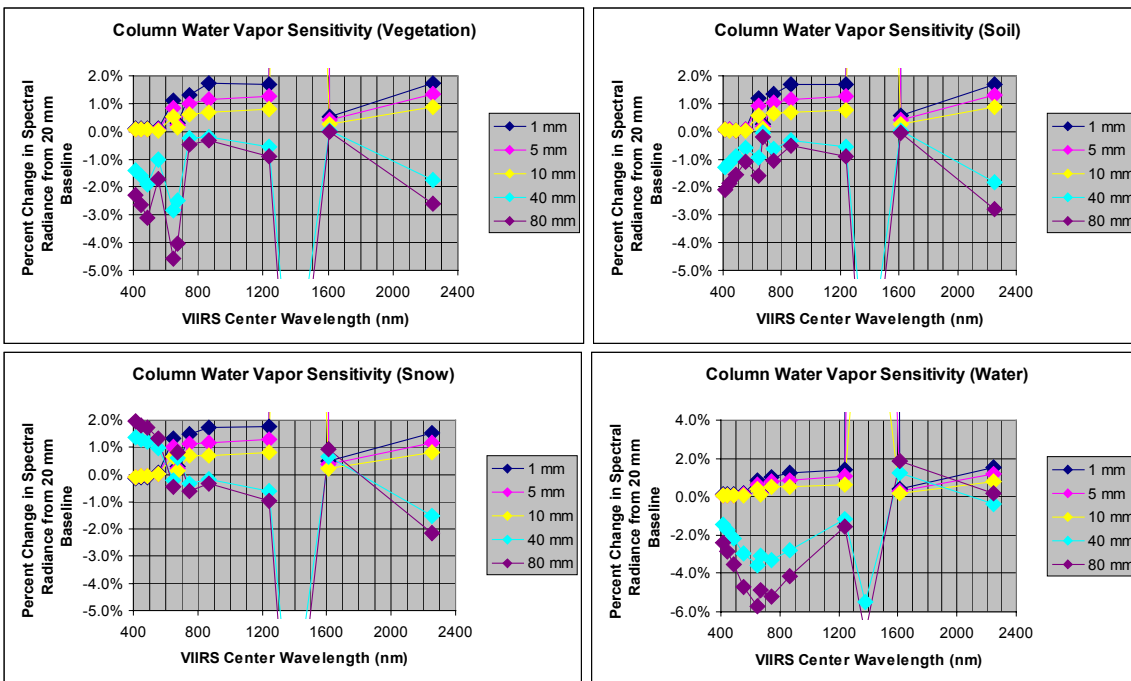
3.4.2.3 Column Water Vapor

Figure 17 shows the sensitivity of VIIRS TOA radiances to variations in column water vapor amount. The baseline column water vapor here is 20 mm. Across the water vapor measurement range, all bands are affected to some degree. For smaller variations, however, the bands most affected are I1, M6, M7, M8, and M11. This validates the decision to include band M5 on VIIRS, to provide data less sensitive to water vapor effects for more demanding products such as Ocean Color/Chlorophyll. Based on these plots and the expected errors in VIIRS Precipitable Water *[Y3251]*, the Surface Reflectance LUT should be robust enough to handle column water vapor variations with even modest grid resolution.

Figure 17. Sensitivity of TOA radiance in VIIRS spectral bands to variations in column water vapor, from MODTRAN 4.0 simulations.

3.4.2.4 Column Ozone

Figure 18 illustrates the sensitivity of the VIIRS reflective band radiances to variations in column ozone, based on Phase II stick modeling with MODTRAN 4.0. The baseline column ozone amount here is 300 Dobson units. As expected, ozone variations have no impact on the SWIR bands. The bands most affected are M4 and I1, which are closest to the primary ozone absorption feature in the visible portion of the spectrum. The plots indicate the variation of TOA radiance with respect to column ozone amount is quite linear, and operational use of the OMPS column ozone product should lead to negligible errors in Surface Reflectance from column ozone variability.

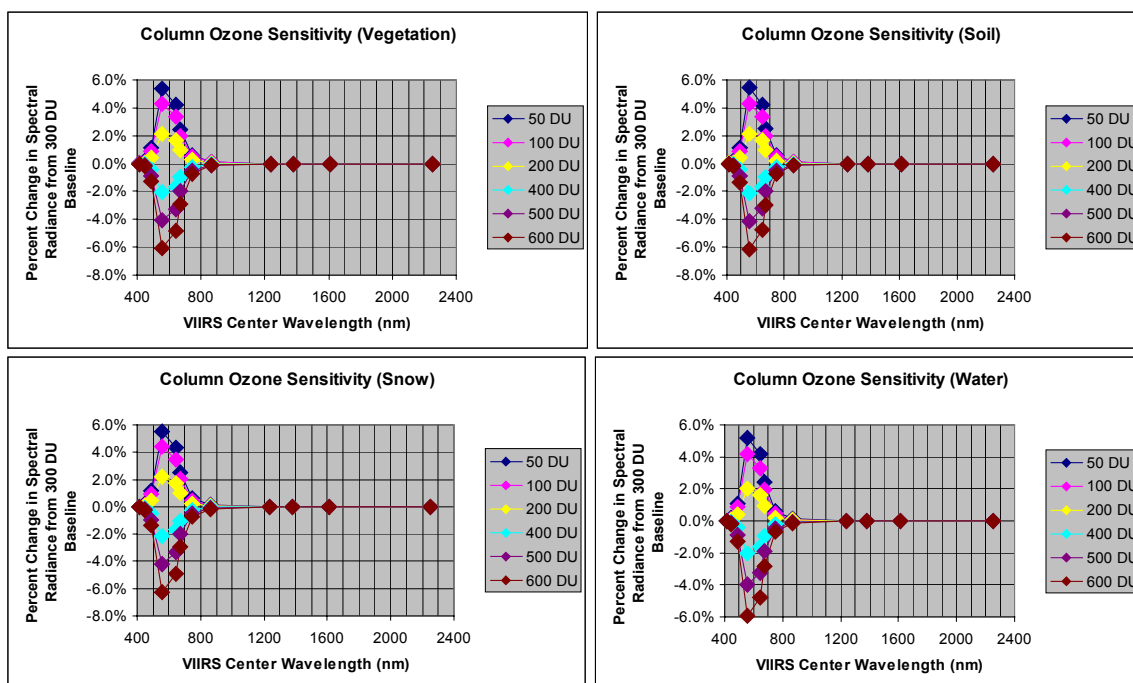**Figure 18. Sensitivity of TOA radiance in VIIRS spectral bands to variations in ozone.**

3.4.2.5 Atmospheric Profile

Figure 19 shows radiance sensitivity to atmospheric type, with column absorbers held constant. A regionally/seasonally based retrieval scheme should be sufficient to minimize these errors.
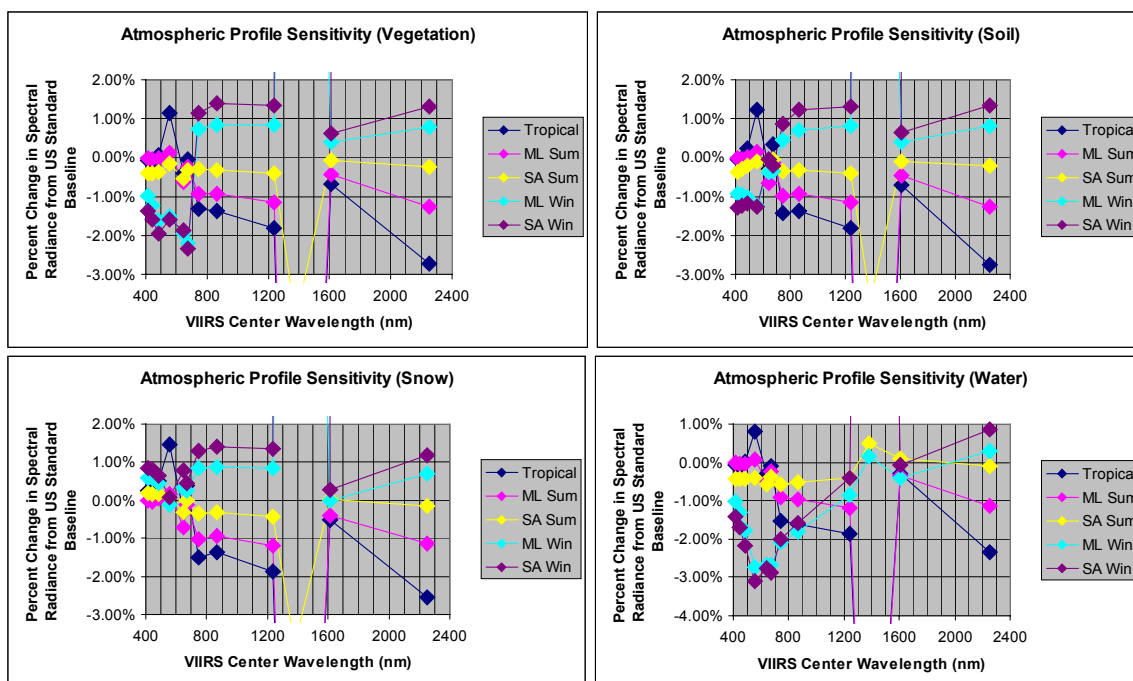

Figure 19. Sensitivity of TOA radiance in VIIRS bands to varying atmospheric profile.

### 3.4.2.6 Tropospheric Aerosol Optical Thickness

Figure 20 and Figure 21 show the errors in surface reflectance encountered when the specification error for the Aerosol Optical Thickness EDR is applied to the input aerosol data, for the Bangladesh and Olympic Peninsula TERCAT scenes, respectively. In both cases, the shortest wavelength bands are the most heavily impacted.   Figure 22 shows the sensitivity of TOA radiance in the VIIRS spectral bands to variations in aerosol optical thickness, for rural aerosols, over four different surface types (vegetation, soil, snow, and water).   The reader should consider the reflectance curves for each surface type, shown in Figure 4 and Figure 5, to place the percentage values of Figure 22 in context.   Larger percentage values tend to occur where the absolute reflectance is lower.   Hence, the percentage variations in TOA radiance for water are relatively large across the spectrum, the percentage variations for vegetation are largest in the realm of chlorophyll absorption, and the percentage variations for snow are largest at 1.6 μm, where snow has a minimum in spectral reflectance.

3.4.2.7 Tropospheric Aerosol Type

Different aerosol models exhibit different phase functions, extinction coefficients, and single scattering albedo, which can alter the effects of a single value of aerosol optical thickness from one type to another. Figure 23 shows the errors introduced by the misclassification of aerosol type before use of the surface reflectance LUT, with continental aerosol as the base type, based on Phase I TERCAT simulations, this time with 6S as the RT model. The differences are noticeable for all misclassifications; the largest errors arise from the differences between the urban model (model #3) and other types available in 6S. Figure 24 shows the sensitivity in TOA radiance for the VIIRS bands, from Phase II simulations with MODTRAN. Here again, urban aerosol seems to cause the largest deviations from the rural baseline for a given optical thickness. Desert aerosol causes significant deviations in the SWIR for surfaces that are dark in these wavelengths.

3.4.2.8 Stratospheric Aerosol Type

Figure 25 shows the sensitivity in TOA radiance for the VIIRS bands to variations in stratospheric aerosol type, in the context of the volcanic models available in MODTRAN 4.0. This RT model characterizes stratospheric aerosol in terms of loading (background, moderate, high, and extreme) and age of the particulates (aged, fresh). The moderate loading parameters are based on more thorough evaluations of real post-eruption data than the high or extreme cases. Except for the extreme loading case, these plots indicate that variation in stratospheric aerosol category as defined here has the same magnitude of impacts on TOA radiance as those for tropospheric aerosol types shown in Figure 24. Volcanic events are not considered typical in an operational sense, but their effects can last several years, and recent eruptions such as Pinatubo have been demonstrated to impact radiative transfer on a global scale.   As a result, it is clear from Figure 25 that the Surface Reflectance LUT must be able to account for variations in stratospheric aerosol. Operationally, the Suspended Matter EDR will indicate the presence of volcanic ash. In the presence of ash sufficient to recategorize stratospheric aerosol from the stratospheric background, a significant portion of the aerosol optical thickness is expected to be due to the stratospheric aerosol. Resolving this with the handling of tropospheric aerosol for the Surface Reflectance LUT is an issue that will be addressed in Version 5 of this document.

Raytheon
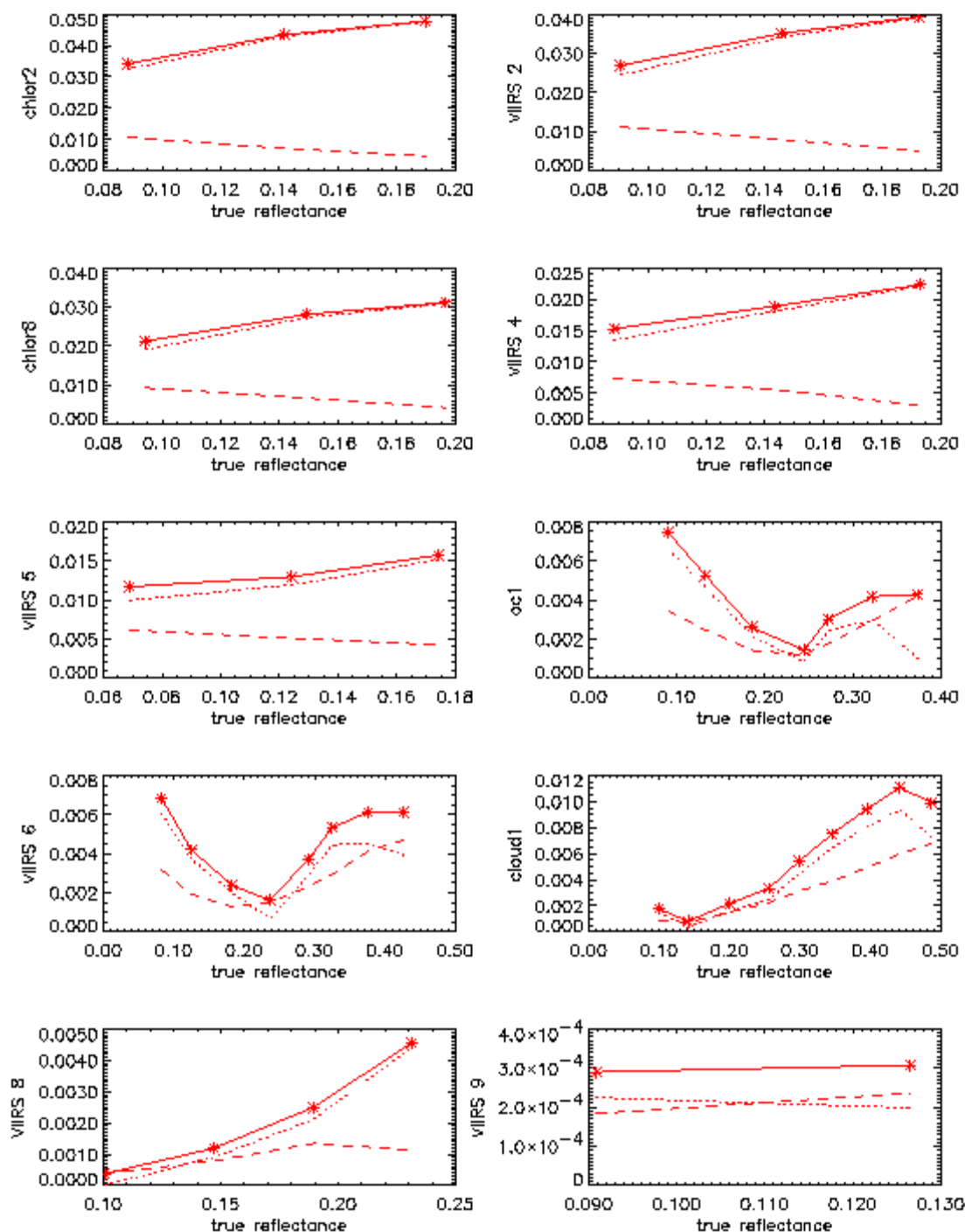
Figure 20. Accuracy (dotted), precision (dashed), and uncertainty (solid) in surface reflectance for 10 VIIRS bands due to spec errors in aerosol optical thickness, for the Bangladesh TERCAT scene. See Table 3 for a mapping of band names in this figure to the new band names.
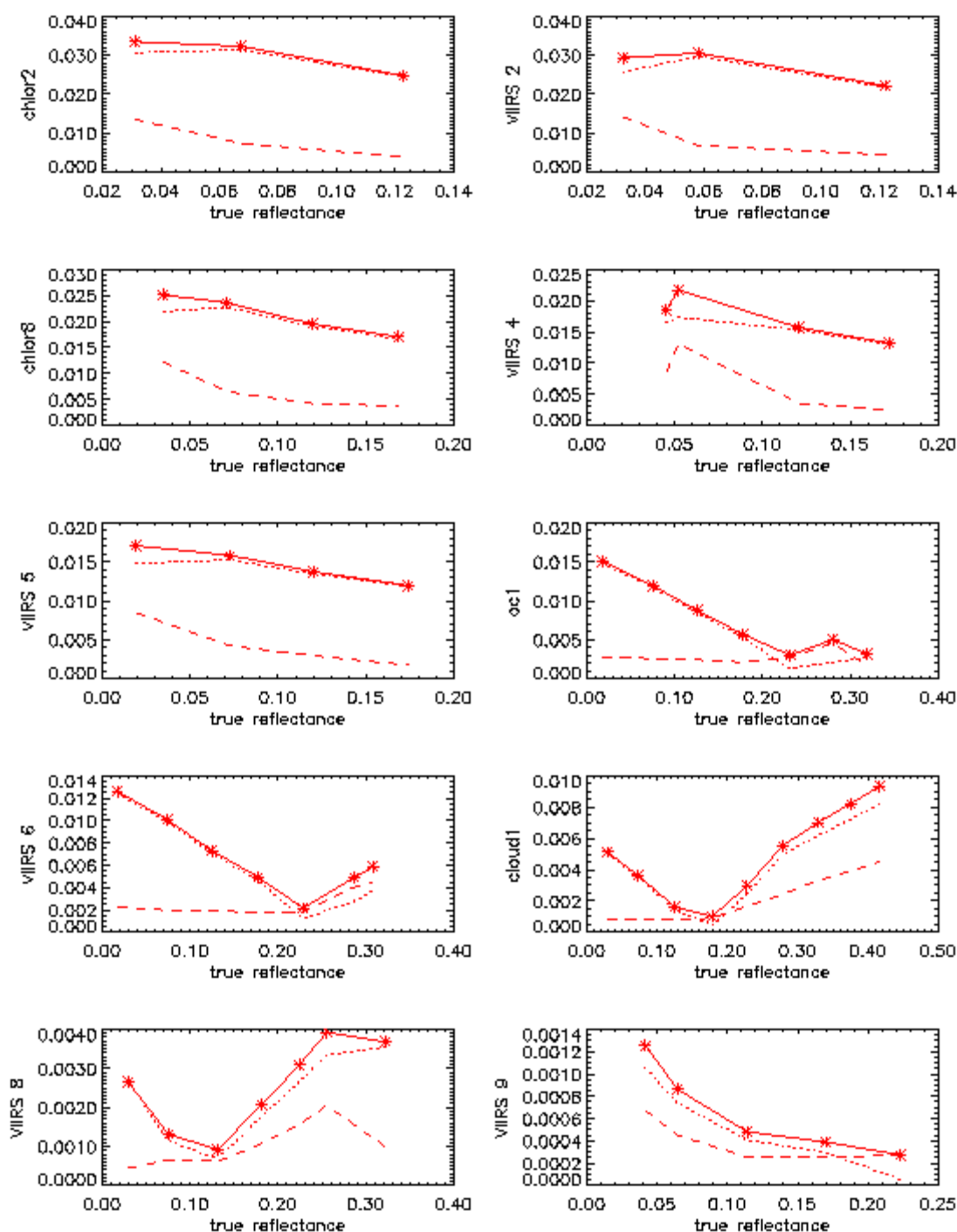
Figure 21. Accuracy (dotted), precision (dashed), and uncertainty (solid) in surface reflectance due to spec errors in aerosol optical thickness, for the Olympic Peninsula TERCAT scene. See Table 3 for a mapping of band names in this figure to the new band names.
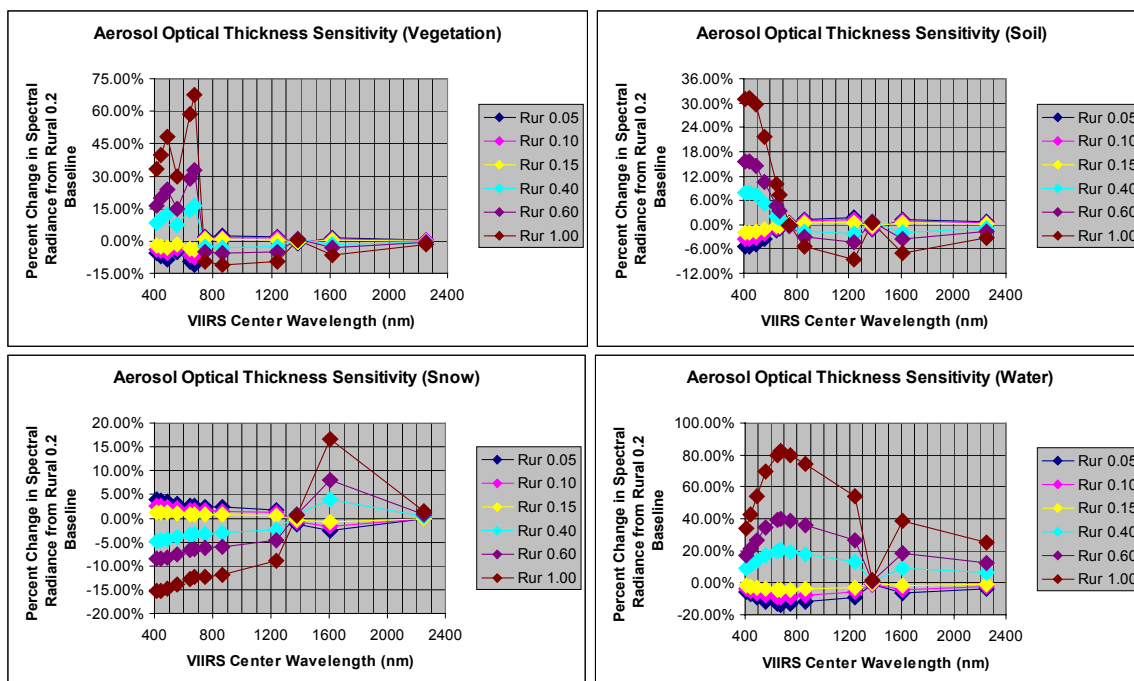
Figure 22. Sensitivity of TOA radiance in VIIRS spectral bands to variations in aerosol optical thickness for rural aerosols, from Phase II MODTRAN simulations.
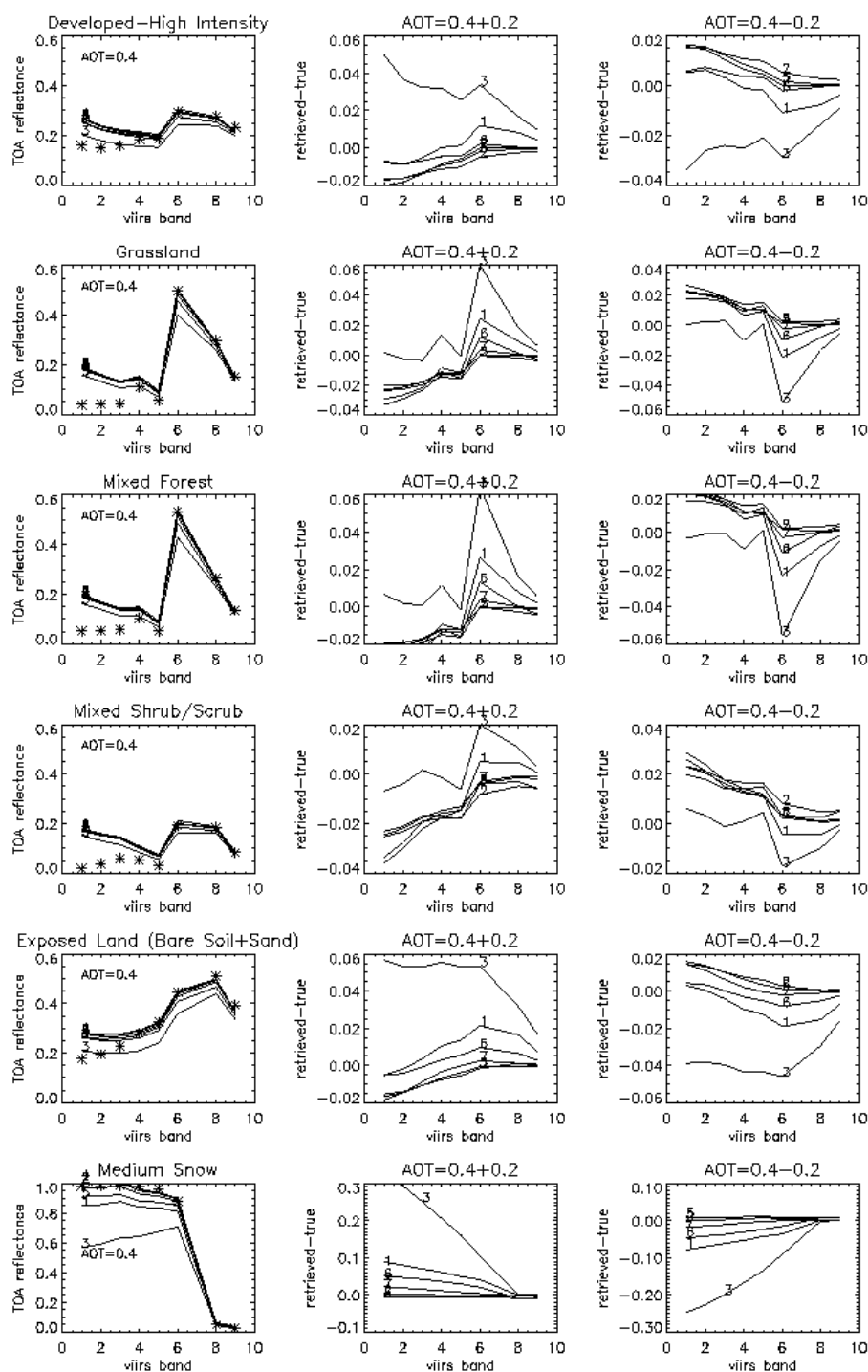
Figure 23. Differences in surface reflectance retrieval caused by misclassification of aerosol type. Column 1 shows TOA reflectance over different land surfaces using the continental aerosol model with AOT=0.4 (rather high). Column 2 shows the differences between retrieved and true surface reflectance resulting from the misclassification.

Figure 24. Sensitivity of TOA radiance in VIIRS spectral bands to variations in tropospheric aerosol type, for an optical thickness of 0.2.

Figure 25. Sensitivity of TOA radiance in VIIRS spectral bands to variations in stratospheric aerosol type as simulated by MODTRAN 4.0.

3.4.2.9 Cirrus Particle Size and Optical Thickness

The initial strategy in Phase I for Surface Reflectance retrievals was to avoid all cloudy pixels. The VIIRS Cloud Mask *[Y2412]*, how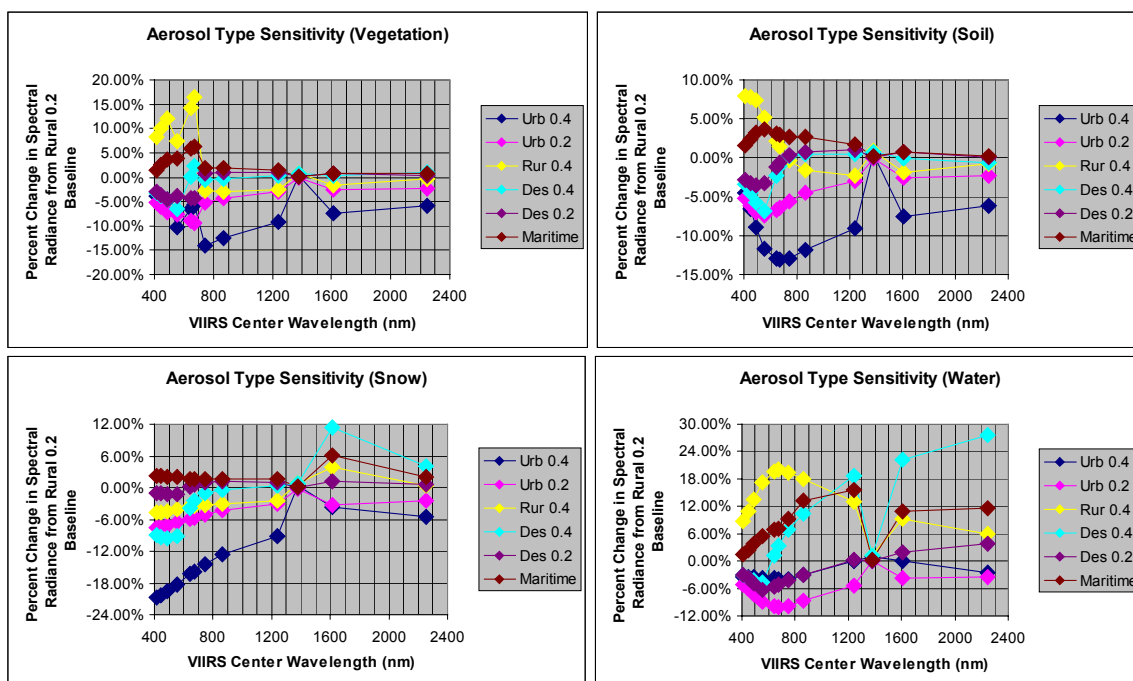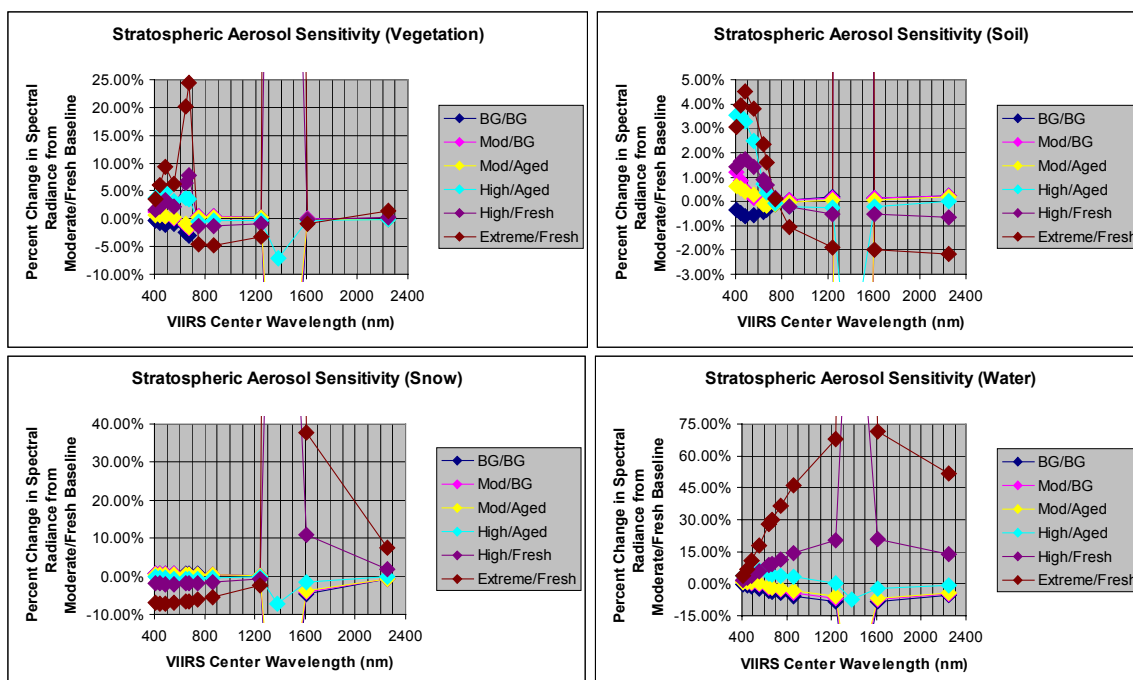ever, building upon MODIS algorithm and hardware capability, will be capable of detecting faint clouds much more effectively than has been possible in the past. Very thin cirrus, which covers a large fraction of the Earth at any given time, will be detectable from VIIRS during the daytime with band M9, which has a demonstrated heritage from MODIS. Often, this cirrus contamination will exhibit an optical thickness equivalent to or less than that of tropospheric aerosol, for which the Surface Reflectance algorithm already performs a correction. The Phase II update to this algorithm has therefore added two dimensions to the Surface Reflectance LUT, namely cirrus particle size and cirrus optical thickness, to expand the global coverage of the Surface Reflectance IP and its downstream products. Operationally, these two LUT inputs will arrive in the form of either the VIIRS Cloud Effective Particle Size and Cloud Optical Thickness EDRs *[Y2393]* or corrections based on VIIRS band M9 (1.38 μm). Figure 26 shows the sensitivity of TOA radiance in the VIIRS spectral bands to variations in cirrus effective particle size (here characterized as a radius), from Phase II stick modeling with MODTRAN 4.0. The baseline cirrus particle radius for the comparisons is 20 μm, and the optical thickness is 0.2, of similar magnitude to typical aerosol optical thickness over land. The percentage variations in the SWIR are consistently higher than in the VNIR, regardless of surface type. In the VNIR, where scattering is the dominant effect of cirrus particles, the larger percentage variations tend to arise for darker absolute reflectances. This is somewhat mitigated in the very short wavelengths by the dominance of Rayleigh scattering. In the SWIR, absorption plays an increasingly larger role for the cirrus particles as the wavelength increases.
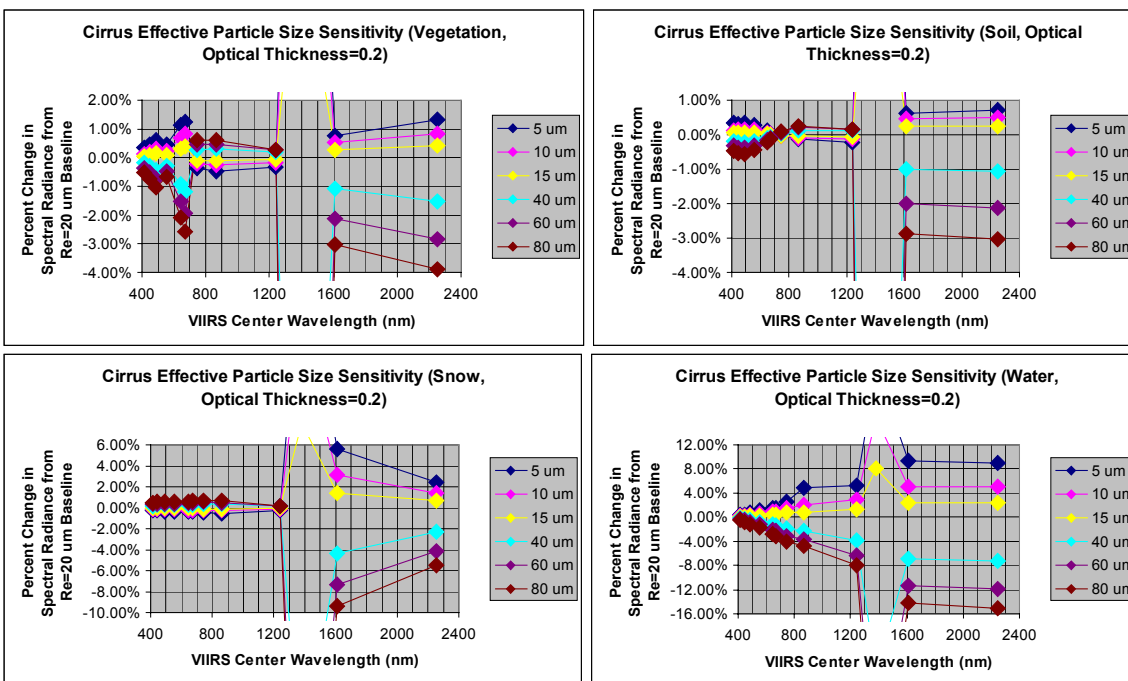
Figure 26. Sensitivity of TOA radiance in VIIRS spectral bands to variations in cirrus particle size, from MODTRAN 4.0 simulations.

It should be noted that MODTRAN 4.0 is not the most ideal model for simulations of cirrus clouds. The internal models were considered unrealistic enough in Phase I to warrant the use of the UCLA model (the reader is directed to *[Y2393]* for a description of this model) for Cloud EDR flowdown and analyses. This is primarily because of the shortcomings in MODTRAN for dealing with the asymmetry of multiple scattering. Additionally, the cirrus cloud parameterization in MODTRAN is not as accurate as that used in the UCLA model. For the top-level simulations being presented here, however, MODTRAN is considered sufficiently accurate to deliver initial guidance on the structure of the LUT. To perform the simulations shown in Figure 26, we used the flexibility of the MODTRAN cumulus cloud parameterization, forcing the cumulus cloud to behave like a cirrus cloud by appropriately setting the height, thickness, and optical properties as a function of wavelength. Because of its flexibility for simulations such as these, we incorporated the parameterization of cirrus optical properties from Key *et al*. (2000), which includes empirically derived formulae for volume extinction, single scattering albedo, and asymmetry as a function of effective radius.

Figure 27 shows the sensitivity of VIIRS TOA radiances to variations in cirrus optical thickness, using similar simulations in MODTRAN 4.0, with an effective particle size of 20 μm and a baseline optical thickness of 0.2. The full scale of sensitivity in M9 is not shown, so that the sensitivity in the other bands can be seen more clearly, but the utility of M9 in detecting thin cirrus is quite apparent from these plots. The behavior with respect to wavelength is very similar to that seen in Figure 26, but on a much larger scale. These plots form the starting point for determining a threshold cirrus optical thickness beyond which retrievals of Surface Reflectance should not be considered reliable, even with a correction applied.
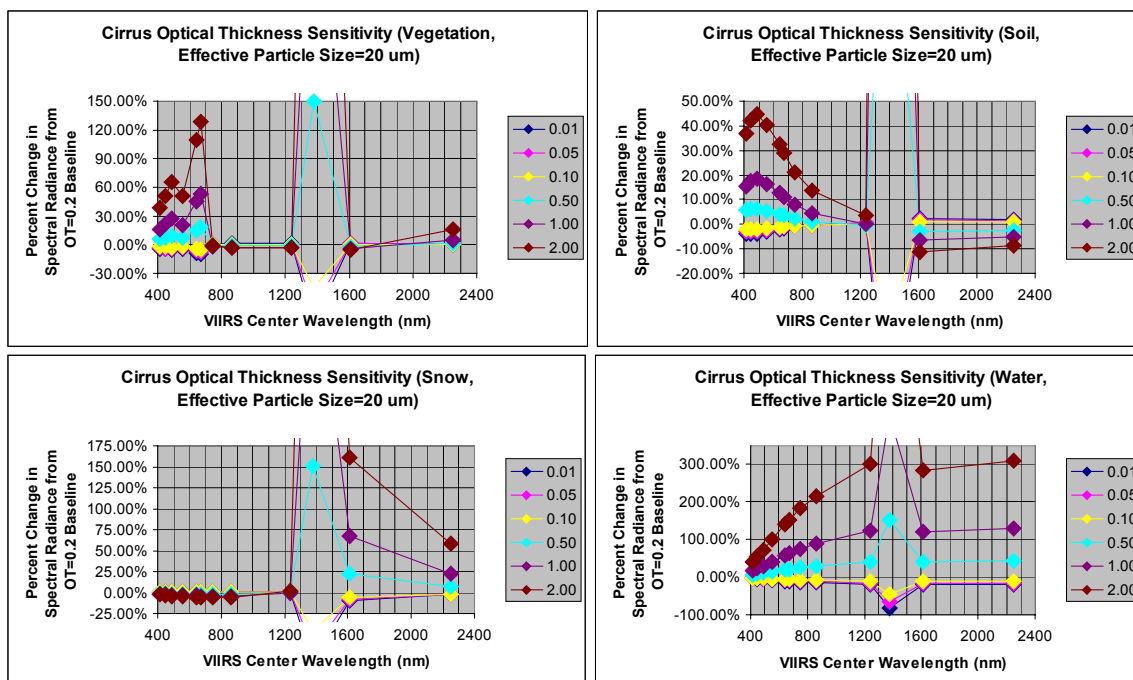
Figure 27. Sensitivity of TOA radiance in VIIRS spectral bands to variations in cirrus optical thickness, from MODTRAN 4.0 simulations.

3.4.2.10 Surface Pressure (Rayleigh Scattering)

Figure 28 shows the sensitivity of the VIIRS reflective bands to variations in surface elevation, with column water vapor and ozone held constant. This is an attempt to explore sensitivity to surface pressure without supplying entirely new atmospheric profiles. The plots therefore provide some degree of insight into the effects of Rayleigh scattering, although water vapor absorption in the compressed profiles will still have a varying effect even with a constant column amount. This is particularly evident in band M11, which should be relatively unaffected by variations in surface pressure alone. But the percentage errors in the shortest wavelength bands reaffirm the importance of the surface pressure dimension in the Surface Reflectance LUT. It is expected, however, that the quality of the inputs from NCEP will be sufficient to make this error small compared to other effects. Further Phase II simulations and analyses will be conducted to confirm this expectation.
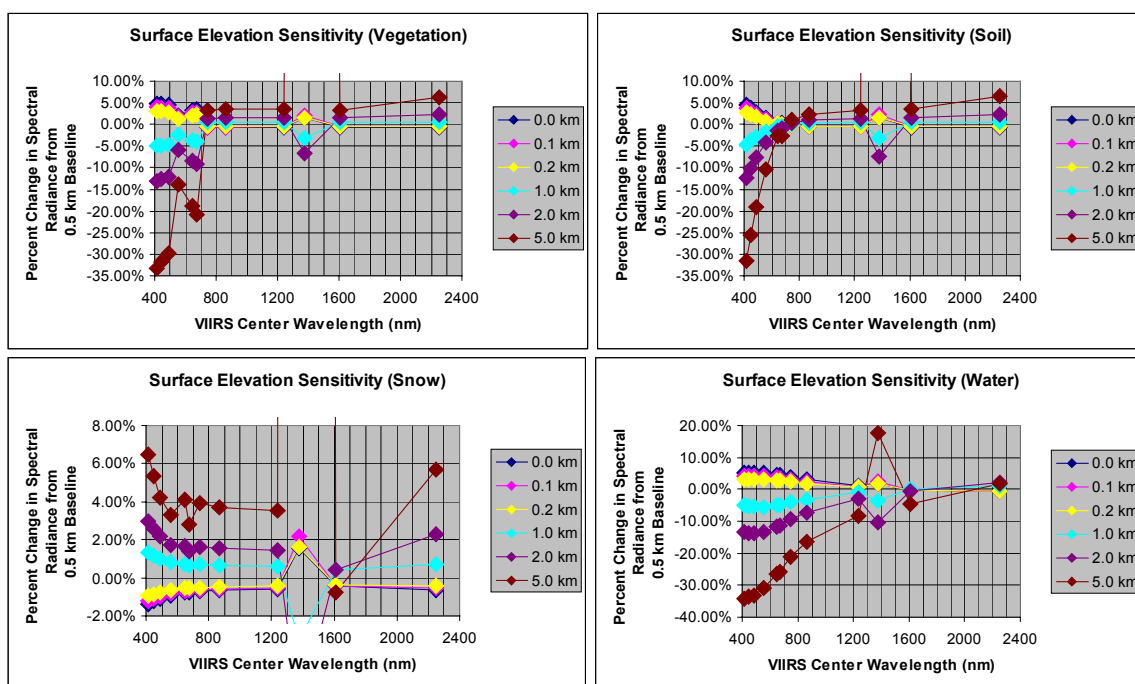
Figure 28. Sensitivity of TOA radiance in VIIRS spectral bands to variations in surface elevation, with column water vapor and ozone held constant.

3.4.2.11 Sensor Noise

In Phase I, Santa Barbara Remote Sensing (SBRS) constructed a detailed radiometric model of the radiometric sensitivity of the VIIRS sensor. This model is initially described in detail in Hucks (1998). It continues to serve as the basis for EDR simulations and performance verification in Phase II. The model describes the sensor noise as a function of TOA band radiance, N_{TOA} as,

$$\sigma = \sqrt{\alpha N_{TOA} + \beta} \qquad (12)$$

where N_{TOA}, a band radiance in units of $Wm^{-2}sr^{-1}$, is chosen as a naming convention to differentiate it from L_{TOA}, the spectral radiance in $Wm^{-2}sr^{-1}\mu m^{-1}$. The quantity σ is the standard deviation of the total sensor noise, assuming a Gaussian distribution. Although this assumption breaks down for very low radiances, it is deemed a sufficiently accurate approximation for the present simulations. The values α and β are two constants derived from the numerous physical quantities associated with sensor noise, including measured detector characterizations, integration time, instantaneous field of view (IFOV), optical throughput, and so forth. In Phase I, we applied these constants as supplied by SBRS for the specified level of sensor noise in the appropriate bands, and the resulting errors are negligible for Surface Reflectance applications, typically on the order of 0.005 reflectance units or less. The only band significantly affected by sensor noise is band I3, an imagery-resolution band in a region of the spectrum where the solar signal is relatively low. Aggregation of this band to moderate resolution, however, cuts the noise in half and renders the band sufficiently sensitive for use by the appropriate algorithms. For snow cover applications, aggregation is not necessary to provide the necessary level of performance. Sensor noise is generally not a significant error source for VIIRS land products, because the VIIRS has been driven to extremely clean radiometric performance by the requirements of the Sea Surface Temperature and Ocean Color/Chlorophyll EDRs.

3.4.2.12 Sensor Calibration

In Phase I, the spec level of 2% calibration error was applied to TOA radiances in our sensitivity studies to determine the magnitude of calibration effects on surface reflectance retrievals. The results for the Olympic Peninsula scene are shown in Figure 29. The high level of calibration performance specified for the VIIRS reflective bands should ensure a healthy continuation of the heritage being developed from MODIS data.
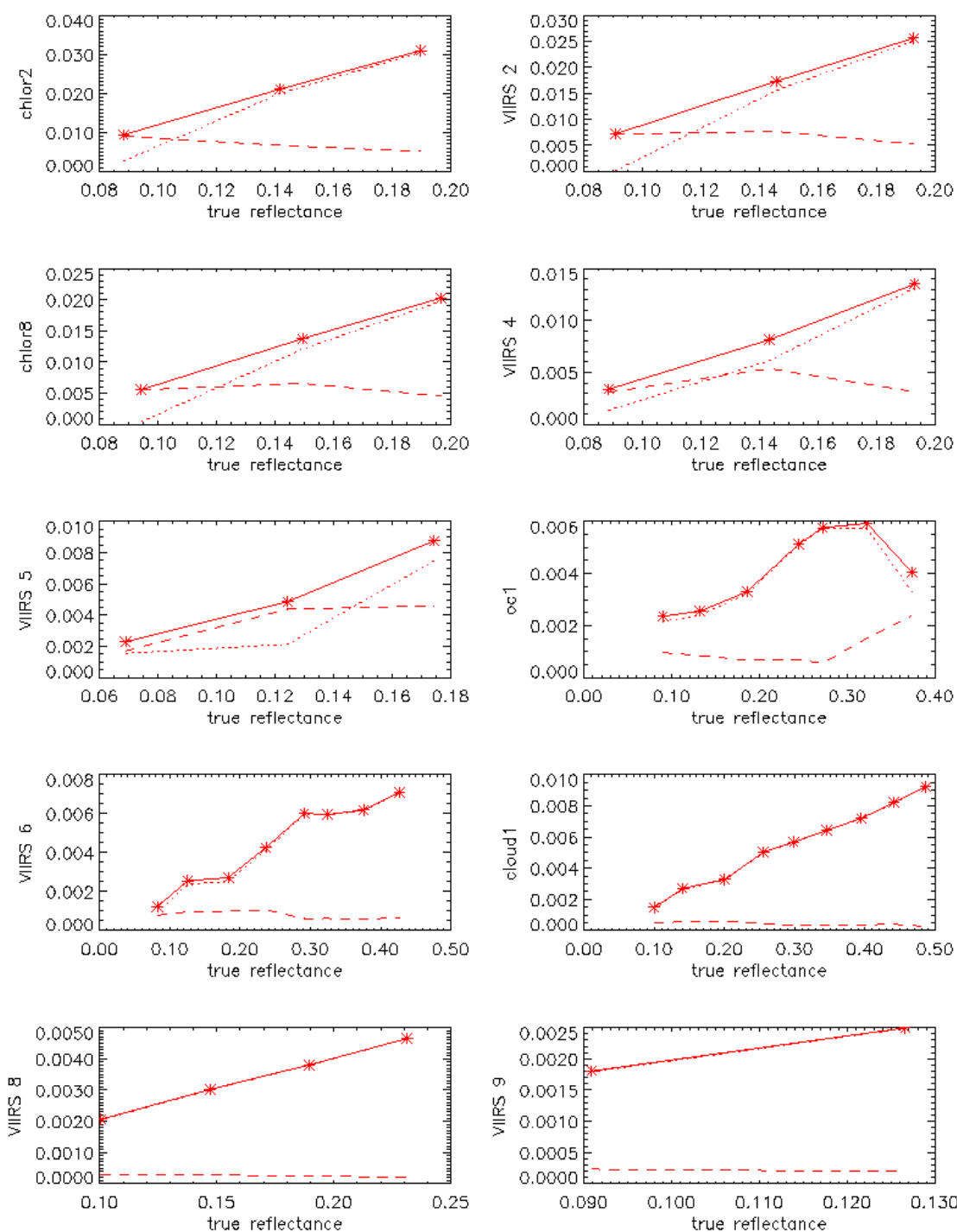
Figure 29. Accuracy (dotted), precision (dashed), and uncertainty (solid) in surface reflectance for ten VIIRS bands, due to calibration error of 2%. See Table 3 for a mapping of band names in this figure to the new band names.

3.4.13 Total Performance Stratification

To arrive at a total measure of performance for Surface Reflectance in Phase I, stick models were generated as described in Section 3.4.1.2. The results of other simulations described in previous sections were used to allocate errors due to temperature, pressure, ozone, water vapor, and forward modeling. Aerosol retrievals were simulated by adding the spec errors for the Aerosol Optical Thickness EDR to the true aerosol values. Calibration biases both up and down were considered, and the sensor specification and predicted performance for both noise and calibration were used to generate the results, which are summarized in Figure 30 through Figure 38, for bands M1, M2, M3, M4, I1 (aggregated 2x2), I2 (aggregated 2x2), M8, I3 (aggregated 2x2), and M11. Plots for unaggregated I1, I2, and I3 will be provided in Version 5 of this ATBD; for the present, it is sufficient to note that the MTF error and misregistration error will be somewhat higher for unaggregated imagery-resolution bands (Phase I analyses suggest each error source increases approximately by a factor of two). The results are stratified by surface type, solar zenith, and view zenith (nadir versus edge of scan). These plots form the basis for the system specification for the Surface Reflectance IP. The predicted performances, based on assessment of margin against sensor calibration and noise performance, have evolved since Phase I, however the associated changes have not yet been incorporated into Phase II results. These will be updated in Version 5 of this document. The plots on the following pages are not intended to guarantee the performances shown under all circumstances, but rather to give a sense of the magnitude of errors in the Surface Reflectance IP for various snapshot conditions.

Figure 30. Stratified spec and predicted performance of the Surface Reflectance IP, at 412 nm (M1).
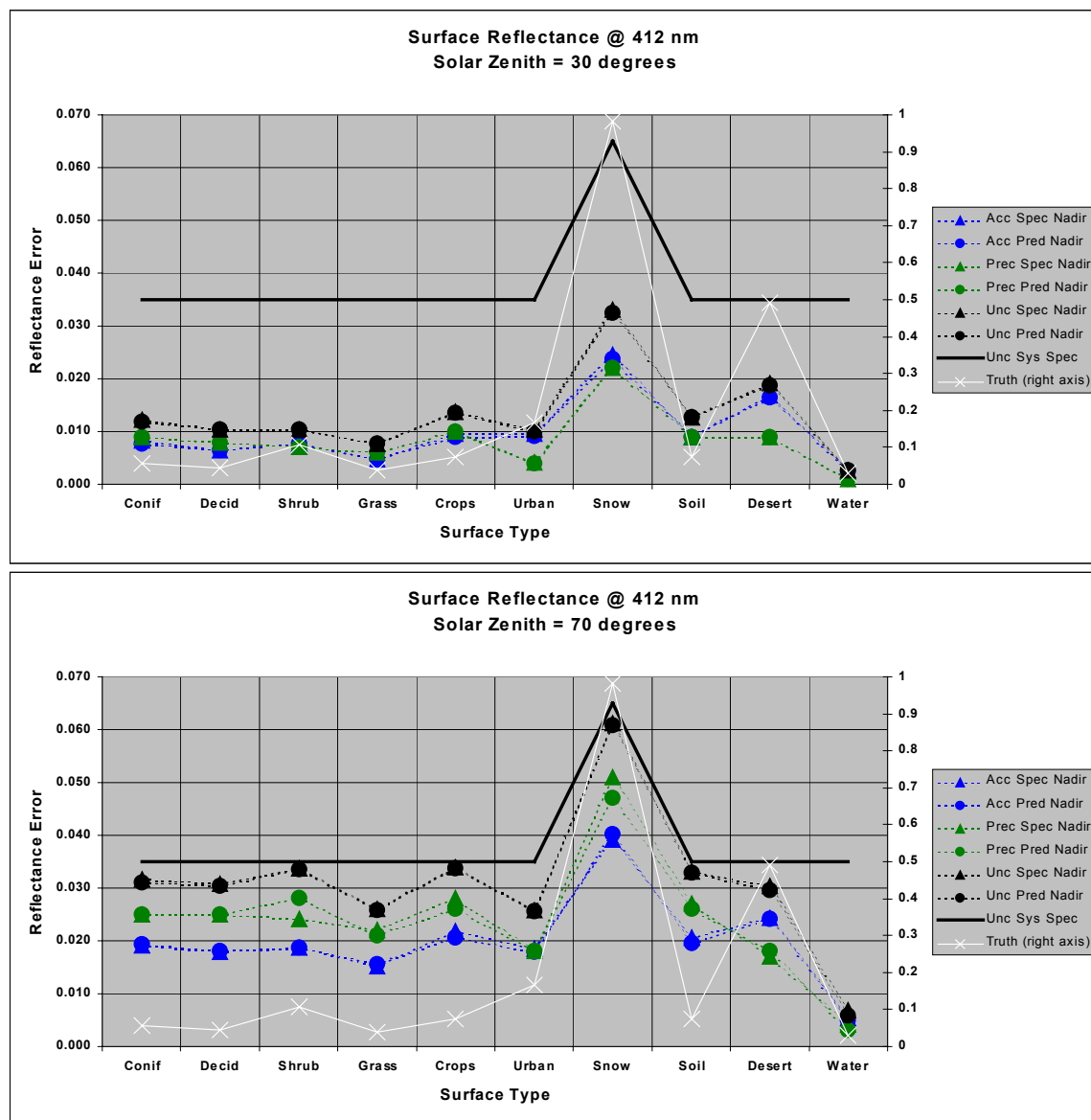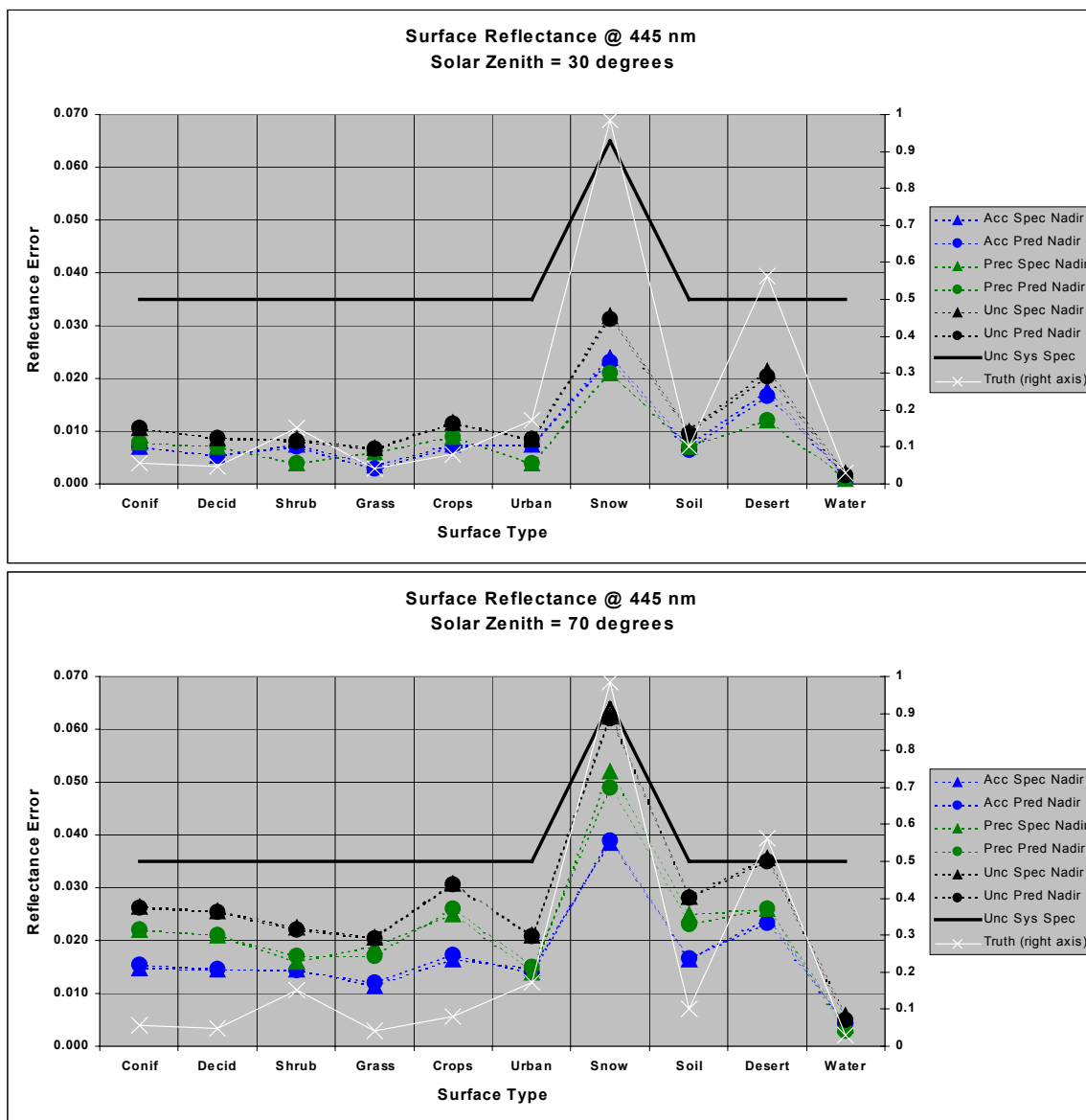
Figure 31. Stratified spec and predicted performance of the Surface Reflectance IP, at 445 nm (M2).

**Figure 32. Stratified spec and predicted performance
of the Surface Reflectance IP, at 488 nm (M3).**
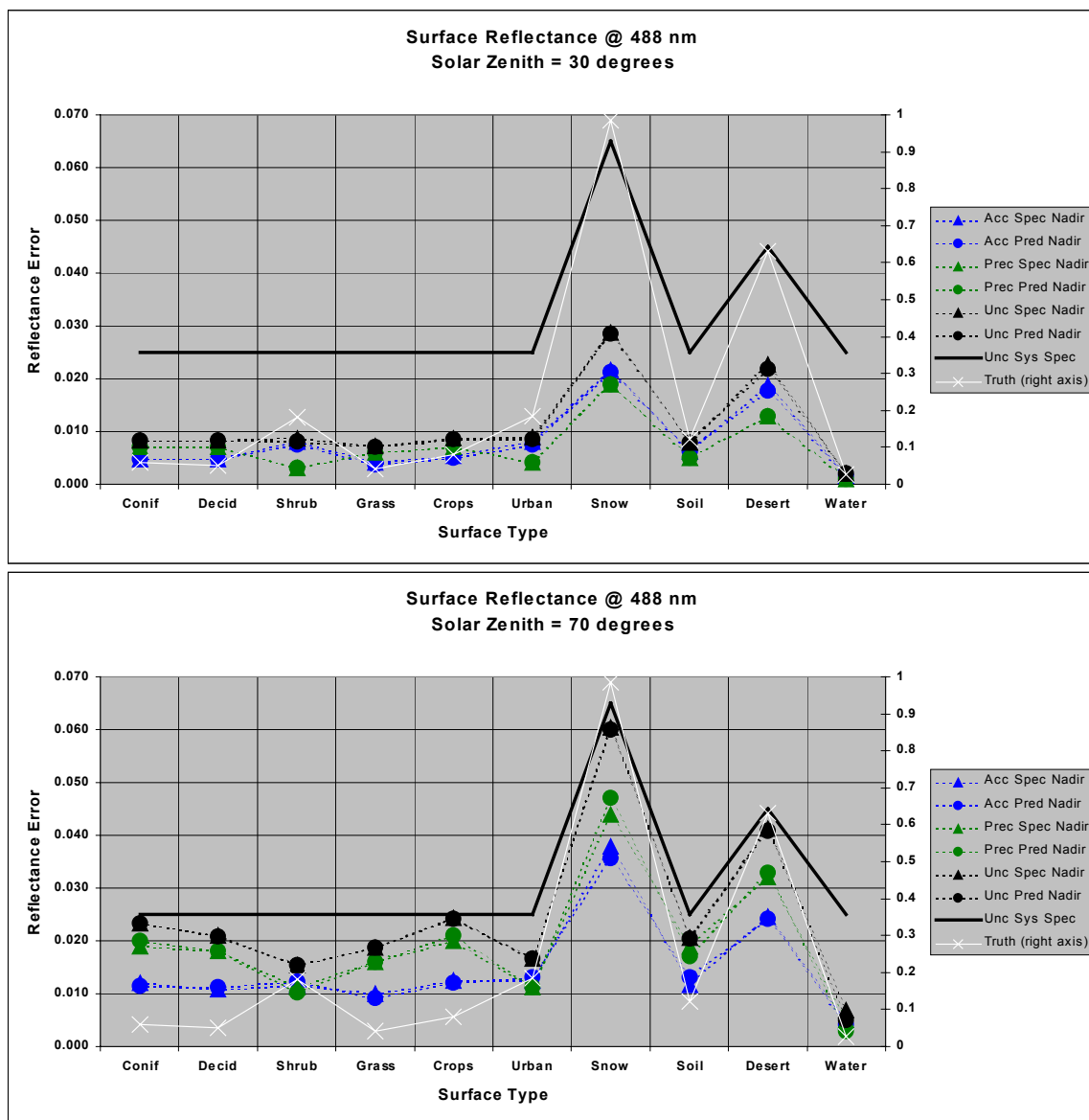
**Figure 33. Stratified spec and predicted performance
of the Surface Reflectance IP, at 555 nm (M4).**

**Figure 34. Stratified spec and predicted performance
of the Surface Reflectance IP, at 645 nm (I1 aggregated 2x2).**

**Figure 35. Stratified spec and predicted performance
of the Surface Reflectance IP, at 865 nm (I2 aggregated 2x2).**

**Figure 36. Stratified spec and predicted performance
of the Surface Reflectance IP, at 1240 nm (M8).**

**Figure 37. Stratified spec and predicted performance
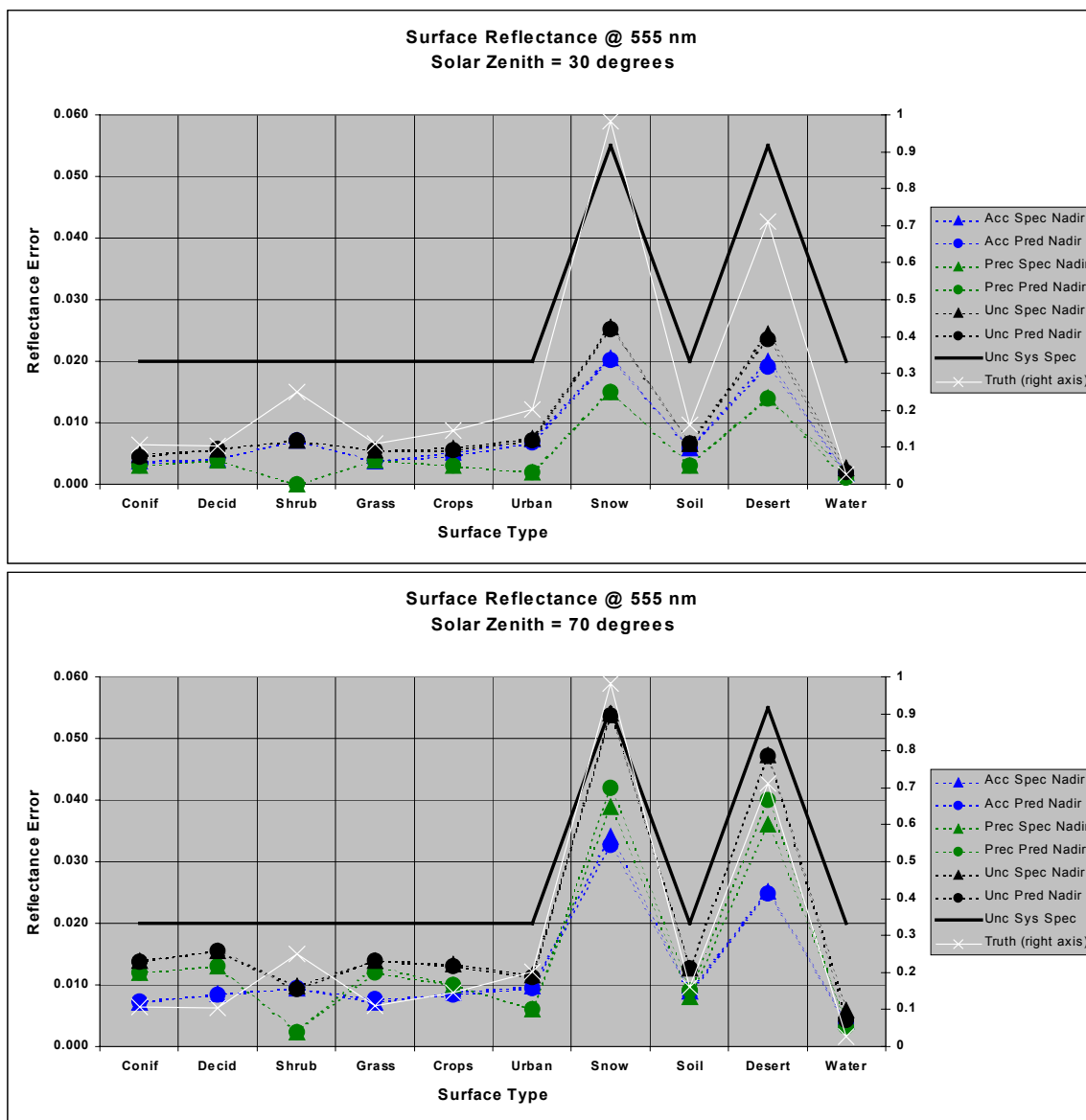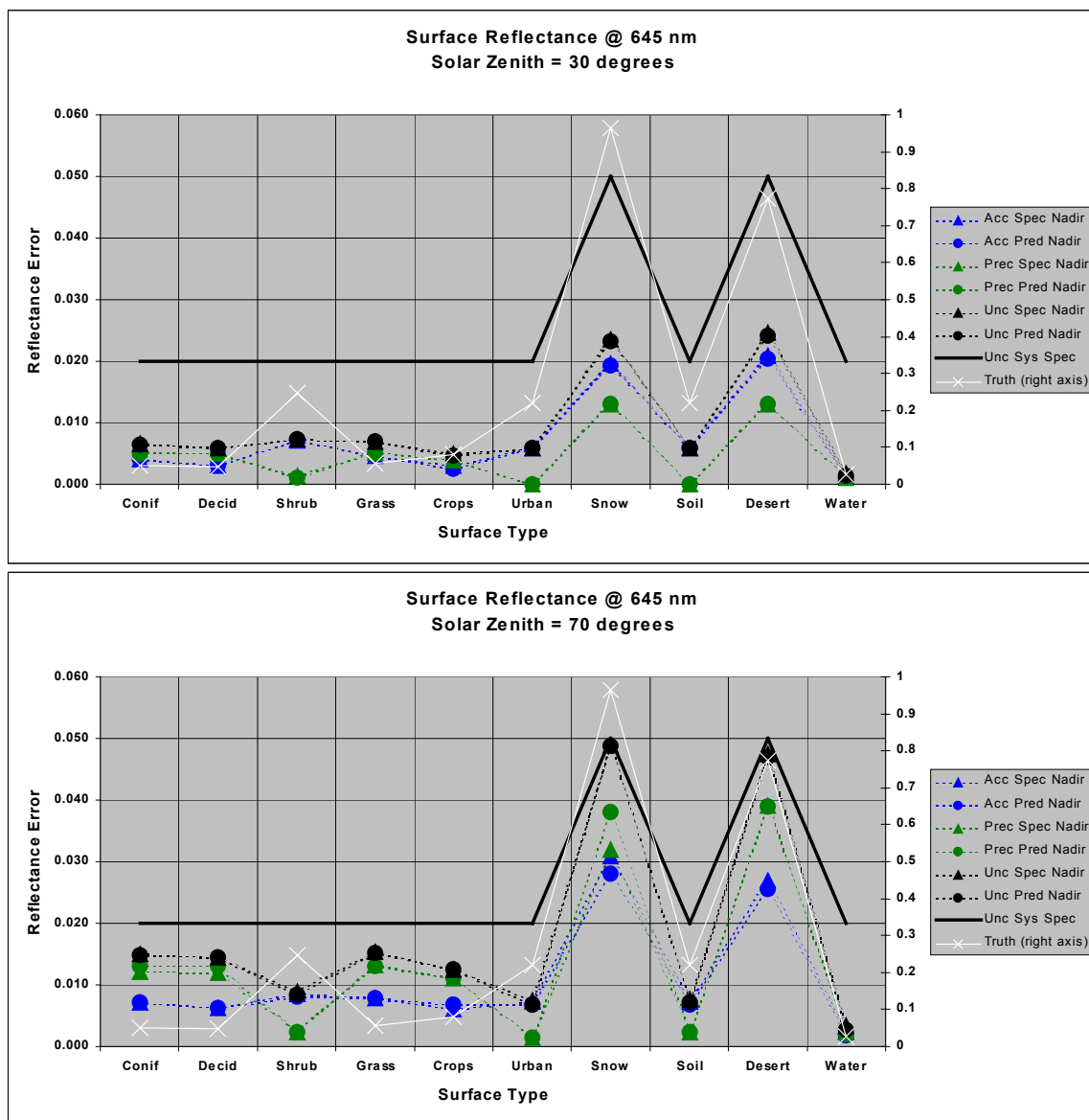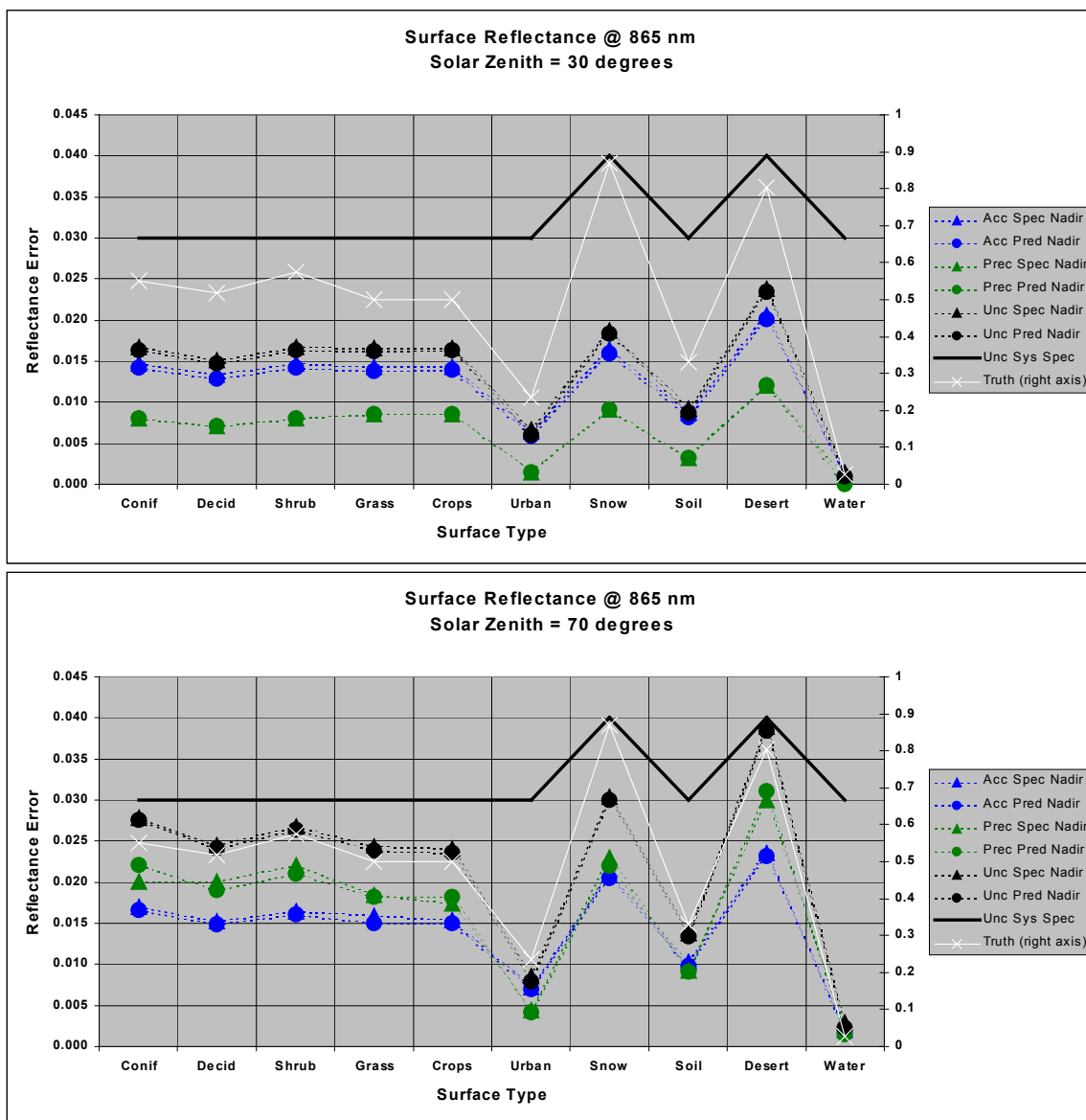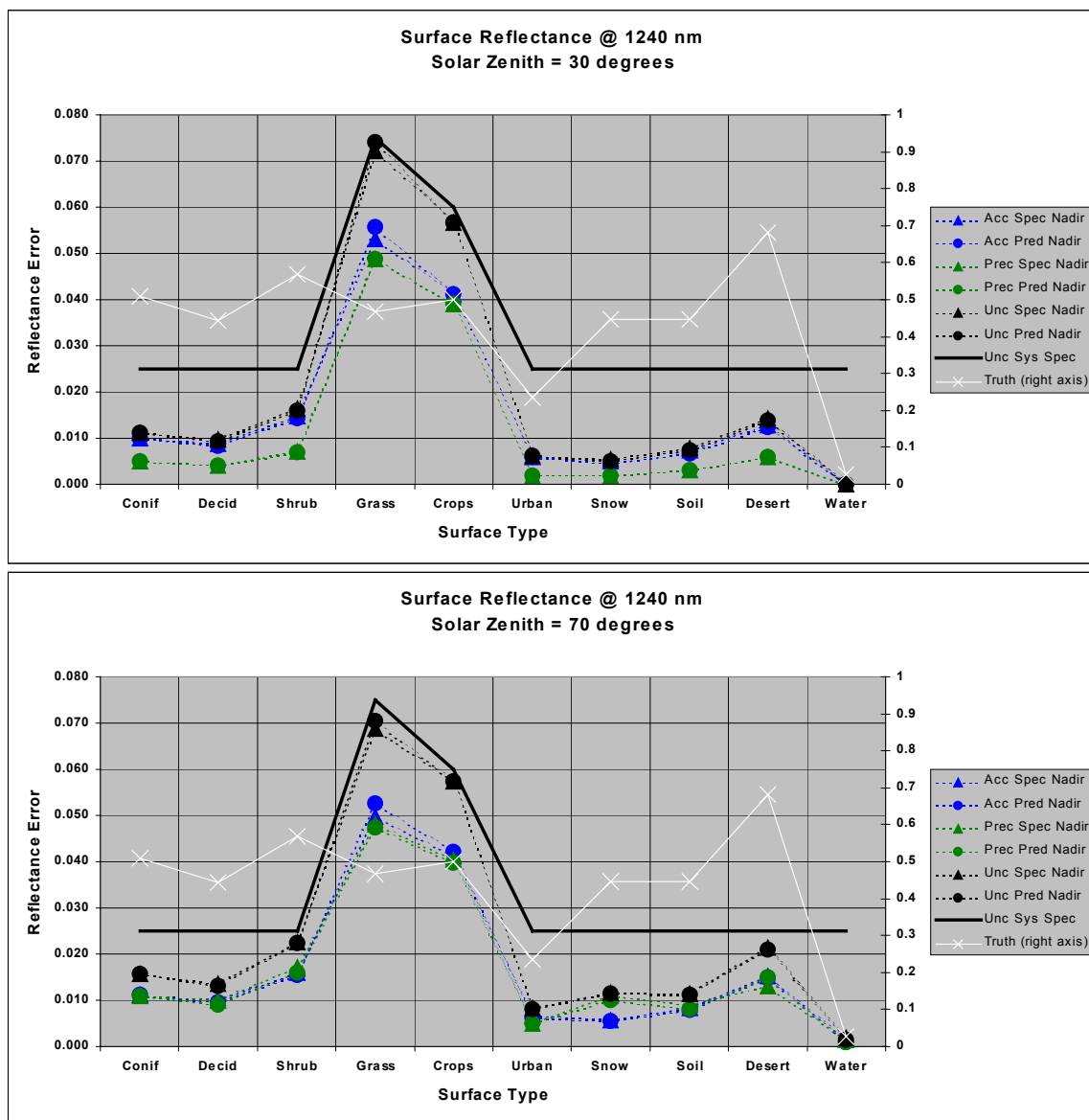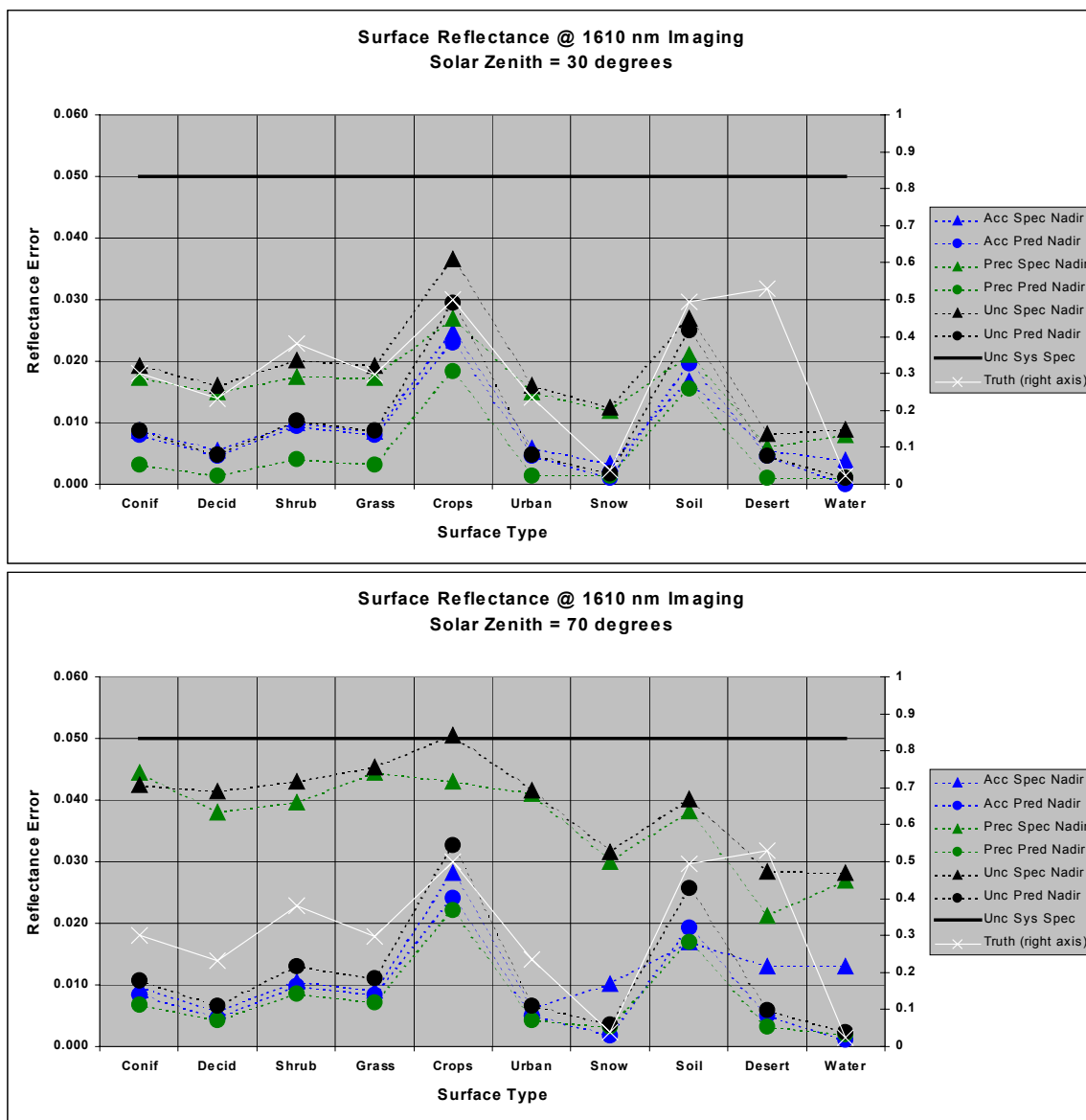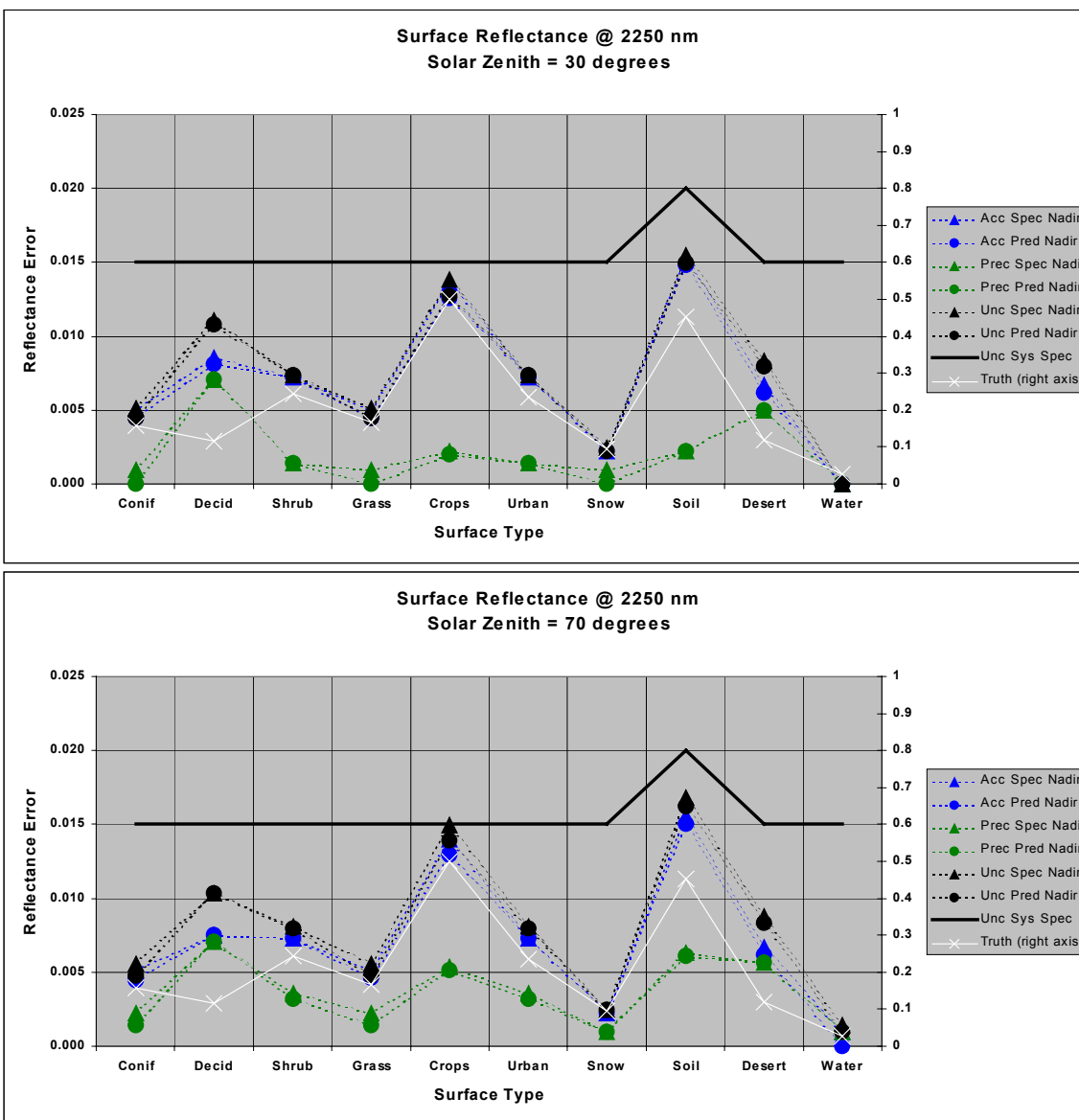of the Surface Reflectance IP, at 1610 nm (I3 aggregated 2x2).**

Figure 38. Stratified spec and predicted performance of the Surface Reflectance IP, at 2250 nm (M11).

3.5   PRACTICAL CONSIDERATIONS

3.5.1   Numerical Computation Considerations

Paragraph SRDV3.2.1.5.4-1 of the VIIRS SRD states the following:

"The scientific SDR and EDR algorithms delivered by the VIIRS contractor shall be convertible into operational code that is compatible with a 20 minute maximum processing time at either the DoD Centrals or DoD field terminals for the conversion of all pertinent RDRs into all required EDRs for the site or terminal, including those based wholly or in part on data from other sensor suites."

RDR here stands for Raw Data Record. This essentially means that any and all EDRs must be completely processed from VIIRS raw data, including calibration and geolocation, within 20 minutes from the time the raw data are available. This requirement is a strong reminder that VIIRS is an operational instrument with real-time user needs.

For the Surface Reflectance IP, even though a LUT approach is being employed, the challenges posed by the SRD timeliness requirement are not trivial. Application of a LUT with as many dimensions as are listed in Table 2 will require the use of advanced programming techniques to minimize search time and I/O. It will also be necessary to break off some dimensions into supplemental LUTs of correction factors or empirical formulae, where possible. Water vapor absorption, atmospheric profile, and column ozone are likely examples of such dimensions. A central task of Phase II, to be summarized in Version 5 of this document, is to determine as completely as possible what the appropriate grid structure and final number of dimensions in the Surface Reflectance LUT should be. But even if some dimensions can be converted to correction factors, it will still be vital to utilize state-of-the-art search and I/O methodologies to ensure the timeliness requirement is not endangered for this pivotal intermediate product. Additionally, this IP is required for a number of downstream products, and so it will require completion far in advance of the 20-minute limit.

Computation time for the weekly and monthly offshoots of Surface Reflectance is not expected to be an issue, as much of this burden can be moved offline. The computations involved are quite straightforward in any event.

3.5.2   Programming and Procedural Considerations

As noted in the previous section, the chief software challenge for Surface Reflectance is to maximize the efficiency of searching the LUT. It will also be important to ensure sufficient memory or storage to hold the LUT at operational processing time. VIIRS Phase II efforts are largely software-focused, and the methodology for this development work is based on sound and proven principles, as discussed in the VIIRS Algorithm Software Development Plan *[Y6635]*. The present maturity of the VIIRS software is detailed in the VIIRS Algorithm Software Maturity Assessment document *[Y6661]*. The maturity and remaining Phase II tasks for the algorithms themselves is summarized in the VIIRS Algorithm/Data Processing Technical Report *[Y7040]*. The software designs relevant to Surface Reflectance are summarized in the VIIRS Context Level Software Architecture *[Y2469]*, Land Module Level Software Architecture *[Y2474]*, Land Module Level Detailed Design *[Y2483]*, and Surface Reflectance IP Unit Level

Detailed Design *[Y2498]*. These designs will be tested at the system level as described in the most recent versions of the VIIRS Software Integration and Test Plan *[Y3236]*, Algorithm Verification and Validation Plan *[Y3237]*, and System Verification and Validation Plan *[Y3270]*. A summary of the ultimate strategy for operational application of the system of VIIRS algorithms is provided in the VIIRS Operations Concept document *[Y2468]*. The VIIRS Interface Control Document (ICD *[Y2470]*) provides more detail on the specifics of ancillary data requirements for Surface Reflectance and other VIIRS products.

3.5.3   Configuration of Retrievals

The primary adjustable parameters for the retrieval of the Surface Reflectance IP are those that govern the overall stratification with respect to the expected quality of the output. These parameters are summarized in Table 5. The values listed may evolve with time leading up to the launch of the VIIRS prototype, and again leading up to the launch of the first operational instrument.

Table 5. Configuration of parameters for Surface Reflectance retrievals.

Symbol	Description	Current Value
θ_{0ques}	Solar zenith angle at which retrievals are flagged as questionable	70°
θ_{0max}	Maximum allowable solar zenith angle	85°
f_{ques}	Threshold non-cirrus cloud fraction within pixel beyond which retrievals become flagged as questionable (probably clear and probably cloudy will be processed along with confident clear, but flagged)	0%
τ_{qaues}	Threshold aerosol optical thickness beyond which retrievals become flagged as questionable	0.5
τ_{cques}	Threshold cirrus optical thickness beyond which retrievals become flagged as questionable	TBD
τ_{amax}	Maximum aerosol optical thickness beyond which retrievals will not be conducted	2.0
τ_{cmax}	Maximum cirrus optical thickness beyond which retrievals will not be conducted	TBD

Another central task of Phase II will be to develop and refine the Land Quality Flag (LQF) structure in detail. This data structure operationally indicates the quality of Surface Reflectance, Vegetation Index, Surface Albedo, Surface Type, Soil Moisture, and Active Fires. It will be summarized at length in Version 5 of this document. The parameters listed in Table 5 form a starting point for the LQF output structure.

3.5.4   Quality Assessment and Diagnostics

Operationally, quality control is automated for the Surface Reflectance IP, using the LQF output. In order to ensure a high level of quality in the product, it is necessary to periodically perform manual inspections of both the input data and the processing scheme. The VIIRS team will use a variety of inputs to this process, including but not limited to surface-generated maps of vegetation cover, albedo, aerial photography and remote sensing of vegetation, data from other

sensors, and statistical analyses. This process will be summarized in detail in Version 5 of this document, along with a description of the LQF output.

3.5.5 Exception Handling

There are a number of situations encountered in practice that will preclude the accurate retrieval of the Surface Reflectance IP. In some instances, the degradation in accuracy is sufficiently small that the products are reported regardless. At other times, the degradation is high enough that retrieval becomes counterproductive. Table 6 summarizes the current sources of exceptions for Surface Reflectance product generations, along with a brief description of the strategy for dealing with each source. If any of these sources is present as a significant contributor to the degradation in the product, the user will be notified via a corresponding flag in the LQF output. The flags will be sufficiently categorized to clearly indicate the suspected source or sources of degradation for a given pixel. These parameters will be refined and described in greater detail in Version 5 of this document.

Table 6. Exception sources and handling strategies for Surface Reflectance retrievals.

Exception Source	Strategy
τ_a beyond τ_{aques}	Report, flag as obscured by aerosol
τ_a beyond τ_{amax}	Do not report, flag as missing
τ_c beyond τ_{acues}	Report, flag as obscured by cirrus
τ_c beyond τ_{cmax}	Do not report, flag as missing
Pixel flagged as confident cloudy, non-cirrus	Do not report, flag as missing
Pixel flagged as probably clear or probably cloudy, non-cirrus	Report, flag as possibly obscured by non-cirrus cloud
Solar zenith angle between θ_{0ques} and θ_{0max}	Report, flag as low illumination
Solar zenith angle higher than θ_{0max}	Do not report, flag as missing
Geolocation unavailable or unreliable	Report, flag as unregistered

3.6 ALGORITHM VALIDATION

Validation requires detailed knowledge of the relationship between measurables and geophysical quantities of interest over the full range of possible conditions. Pre-launch activities include determination of algorithms and characterization of uncertainties resulting from parameterizations and their algorithmic implementation. Post-launch activities include refinement of algorithms and uncertainty estimates based on near-direct comparisons with correlative data and selected, controlled analyses.

3.6.1 Pre-Launch Algorithm Test/Development Activities

Pre-launch algorithm and system performance validation will be performed primarily with MODIS data, as the spectral bands are very similar and in many cases identical to those for VIIRS. The algorithm heritage is also quite similar for the two systems. The MODIS validation infrastructure, combined with international cooperative efforts such as Long Term Ecological

Research (LTER) and the Global Terrestrial Observing System (GTOS), will allow for rigorous validation without high cost or risk. Existing data sets have already played a role and will continue to do so; an example would be the AVHRR and Thematic Mapper (TM) data collected in the Boreal Ecosystem/Atmosphere Study (BOREAS) to retrieve surface reflectances. The atmospheric inputs can be obtained from *in situ* measurements made during the field campaigns such as BOREAS. For example, aerosol optical thickness (AOT) can be obtained from sun-photometer observations made by the Aerosol Robotic Network (AERONET); the atmospheric conditions will be obtained from other *in situ* measurements or climatological data sets. By comparing those retrieved surface reflectances with other multi-angular airborne measurements (Polarization and Directionality of the Earth's Reflectances [POLDER], Advanced Solid-state Array Spectroradiometer [ASAS]), Portable Apparatus for Rapid Acquisition of Bidirectional Observations of Land and Atmosphere (PARABOLA) measurements, and albedo measurements, we will address the accuracy, uncertainty, and precision of the retrieved surface reflectances at different cases, e.g., their dependencies on the angular sampling, surface conditions, and seasonal changes (for example, snow and no-snow background conditions).

3.6.2   Post-Launch Algorithm Test/Development Activities

Post-launch algorithm and system performance validation/verification will exist as a continuation of the activities formulated and applied pre-launch. Focus will be placed on leveraging existing infrastructures for validation, not just from MODIS activities, but rather on a global scale. Significantly more detail on recommendations for post-launch validation of Surface Reflectance will be provided in Version 5 of this document, once the LUT structure has been nailed down more explicitly.

4.0 ASSUMPTIONS AND LIMITATIONS

4.1 ASSUMPTIONS

This ATBD has included the following assumptions:

1. The applicability and validity of 6S and MODTRAN across the range of solar zenith and viewing zenith limits, cirrus and aerosol properties, and gaseous absorber amounts considered therein

2. The availability of necessary non-VIIRS input data for operational retrievals to the quality described in the VIIRS Interface Control Document *[Y2470]*

3. The availability of an aerosol climatology where aerosol retrievals cannot be performed directly over a large region

4. The feasibility of a software solution to safely fit the Surface Reflectance LUT implementation into the VIIRS timeliness requirements

4.2 LIMITATIONS

Under conditions of extreme aerosol loading, such as that associated with biomass burning, local volcanic eruptions, or other similar events, performance is not guaranteed. Performance is also not guaranteed beyond a TBD level of thin cirrus contamination, or below a TBD level of solar illumination, pending the incorporation of spherical radiative transfer modeling in the generation of the Surface Reflectance LUT.

Raytheon

5.0   REFERENCES

Berk, A., G. P. Anderson, P. K. Acharya, J. H. Chetwynd, L. S. Bernstein, E. P. Shettle, M. W. Matthew, and S. M. Adler-Golden (1999). *MODTRAN4 User's Manual*. Air Force Research Laboratory, Space Vehicles Directorate, Hanscom AFB, MA 01731-3010.

Chandrasekhar, S. (1960). *Radiative Transfer*. New York: Dover.

Fraser, R. S., R. A. Ferrare, Y. J. Kaufman, B. L. Markham, and S. Mattoo (1992). Algorithm for atmospheric corrections of aircraft and satellite imagery. *Int. J. Remote Sensing*, 13(3), 541-557.

Holben, B., E. Vermote, Y. J. Kaufman, D. Tanré, and V. Kalb (1992). Aerosol retrieval over land from AVHRR data-application for atmospheric correction. *IEEE Transactions on Geoscience and Remote Sensing,* 30, 212-222.

Hucks, J. (1998). VIIRS Testbed sensor modeling efforts, Phase I. Raytheon Systems Company Internal Memorandum Y1629.

IPO (2000). Visible/Infrared Imager/Radiometer Suite (VIIRS) Sensor Requirements Document (SRD) for National Polar-Orbiting Operational Environmental Satellite System (NPOESS) spacecraft and sensors, Rev. 3. Prepared by Assoc. Directorate for Acquisition, NPOESS Integrated Program Office, Silver Spring, MD.

Key, J. R., P. Yang, B. A. Baum, S. L. Nasiri (2000). Parameterization of shortwave ice cloud optical properties for various particle habits. Submitted to *Journal of Geophysical Research*.

Kneizys, F.X., L.W. Abreu, G.P. Anderson, J.H. Chetwynd, E.P. Shettle, A. Berk, L.S. Bernstein, D.C. Robertson, P. Acharya, L.S. Rothman, J.E.A. Selby, W.O. Gallery, and S.A. Clough (1996). *The MODTRAN 2/3 Report and LOWTRAN 7 Model*. L.W. Abreu and G.P. Anderson, eds. Prepared by Ontar Corporation, North Andover, Massachussets, for Phillips Laboratory, Geophysics Directorate, Hanscom AFB, Massachussets.

Lee, T. Y., and Y. J. Kaufman (1986). Non-Lambertian effects on remote sensing of surface reflectance and vegetation index. *IEEE Transactions on Geoscience and Remote Sensing,* GE-24, 699-708.

Leroy, M., J. L. Deuzé, F. M. Bréon, O. Hautecoeur, M. Herman, J. C. Buriez, D. Tanré, S. Bouffies, P. Chazette, and J. L. Roujean (1997). Retrieval of atmospheric properties and surface bidirectional reflectances over land from POLDER/ADEOS. *Journal of Geophysical Research,* 102(D14), 17,023-17,037.

Liang, S., H. Fallah-Adl, S. Kalluri, J. JáJá, Y. J. Kaufman, and J. R. G. Townshend (1997). An operational atmospheric correction algorithm for Landsat Thematic Mapper imagery over land. *Journal of Geophysical Research*, 102(D14), 17,173-17,186.

Lyapustin, A. I. (1999). Atmospheric and geometrical effects on land surface albedo. *Journal of Geophysical Research,* 104, 4127-4144.

Lyapustin, A. I., and Y. J. Kaufman (2001). The role of adjacency effect in the remote sensing of aerosol over land. Submitted to *Journal of Geophysical Research*.

Myneni, R. B., and G. Asrar (1994). Atmospheric effect and spectral vegetation indices. *Remote Sensing of Environment*, 47, 390-402.

Ni, W., X. Li, C. E. Woodcock, M. Caetano, and A. Strahler (1998). An analytical model of bidirectional reflectance over discontinuous plant canopies. *IEEE Transactions on Geoscience and Remote Sensing* (in press).

Tanré, D., B. Holben, and Y. J. Kaufman (1992). Atmospheric correction algorithm for NOAA–AVHRR products: Theory and application. *IEEE Transactions on Geoscience and Remote Sensing*, 30, 231-248.

Vermote, E. F., and A. Vermeulen (1999). Atmospheric correction algorithm: spectral reflectances (MOD09). Version 4.0. Algorithm technical background document. *NASA EOS-1D 2015 Doc.*

Vermote, E. F., D. Tanré, J. L. Deuzé, M. Herman, and J-J Morcrette (1997). Second Simulation of the Satellite Signal in the Solar Spectrum, 6S: An Overview. *IEEE Transactions on Geoscience and Remote Sensing,* 35, 675-686.

Raytheon